8-2021

Applications of Vanadium Phthalocyanine in Catalytic, Acid-Based Medium to Couple Sugar Molecules

Juan Ricardo Luna
The University of Texas Rio Grande Valley

APPLICATION OF VANADIUM PHTHALOCYANINE IN CATALYTIC, ACID-BASED MEDIUM TO COUPLE SUGAR MOLECULES

A Thesis

by

JUAN RICARDO LUNA

Submitted to the Graduate College of
The University of Texas Rio Grande Valley
In partial fulfillment of the requirements for the degree of

MASTER OF SCIENCE

August 2021

Major Subject: Chemistry

APPLICATION OF VANADIUM PHTHALOCYANINE IN CATALYTIC, ACID-BASED MEDIUM TO COUPLE SUGAR MOLECULES

A Thesis
by
JUAN RICARDO LUNA

COMMITTEE MEMBERS

Dr. Jason G. Parsons
Chair of Committee

Dr. Arnulfo Mar
Committee Member

Dr. Erik Plata
Committee Member

Dr. Jose J. Gutierrez
Committee Member

August 2021

ABSTRACT

Luna, Juan Ricardo, Applications of Vanadium Phthalocyanine in Catalytic, Acid-Based Medium to Couple Sugar Molecules. Master of Science (MS), August, 2021, 64 pp., 11 tables, 44 figures, references, 32 titles.

The vanadium-substituted tetraazatetrabenzoporphyrin, vanadium phthalocyanine, was synthesized via reflux and characterized using FITR and XRD analysis. Subsequent to synthesis, the vanadium phthalocyanine was studied as a catalyst in redox reactions to convert fructose to different molecules, the products were predominately levulinic methyl ester and heptadionic acid. The ability to convert fructose to other compounds, such as alkyl levulinic derivative, is an important process to help eliminate reliance on traditional chemical feed stocks and promote alternative fuels. Levulinic acid has been commonly used as a starting material in the synthesis of biofuels and a precursor for pharmaceuticals, plasticizers, THF derivatives, γ-valerolatone. In the present study reactions were performed under acidic conditions using strong acids, which included nitric, sulfuric, hydrochloric, and hydrobromic acids, open atmospheric reflux in methanol and the reaction products were analyzed using GC-MS. Levulinic methyl ester and heptadionic acid were identified along with other coupled carbon-carbon products resulting from the de-cyclization of the sugar and subsequent coupling in a single pot reflux. The reactions show that metal-porphyrin systems are catalytic in the generation of organic molecules from biological material such as sugars, cellular material and cell walls.

DEDICATION

I would not have achieved or been given great opportunities in my life if it were not for the continued support of my loved ones. I have been blessed with a loving fiancé, great parents, one-of-kind brother and irreplaceable friends. I owe a great amount of gratitude to Janette Saldana because without her love and encouragement my academic career would not have been a reality today. I am proud to share this and future achievements with my vast family as a symbol of resilience coming from our background. Finally, my grandmother, Maria Micaela Cruces, foresaw and believed in me before I had achieved anything.

ACKNOWLEDGMENTS

I have a great amount of respect and gratitude for my mentors, Dr. Jason Parsons and Helia Morales. Helia Morales was the first professor to motivate me to pursue research and got me going to lab. Without her catalyzing my enthusiasm for research, my achievements would have not begun or continued into further endeavors. For that, I am extremely thankful for the assistance, patience and continued support. Upon his arrival to the Brownsville campus, Dr. Parsons began refining my skills, encouraging my curiosity and supporting my research efforts. His knowledge and view on chemistry concepts has pushed my understanding to heights unobtainable on my own. Due to both their efforts and investment in my education, I will be continuing my career to achieve a doctoral in chemistry.

I would like to give thanks to my thesis committee members: Dr. Arnulfo Mar, Dr. Erik Plata and Dr. Jose Gutierrez. Your time, advice and guidance are greatly appreciated thru my thesis preparations. Including my committee, I am thankful for all the education, interactions and memories the UTRGV chemistry department staff has given me, especially Vanessa Garcia and Dr. Justin Moore. I will carry them into the next chapter of my life.

Finally, I am grateful for my lab colleagues from past and present semesters. Alexis Echevarria and Joe Lara have bounced ideas and progressed our research through many blockades faced together. I will always have fond memories with Kenny, Caro, Alex, Christian, JP, Danny, Douglas, Kevin, and Valeria.

TABLE OF CONTENTS

LIST OF TABLES

LIST OF FIGURES

CHAPTER I

BACKGROUND

Porphyrins and discovery of phthalocyanine

Porphyrins are identified as highly π-conjugated macrocycle molecules consisting of four subunits conjoint by bridges and exist in the metal substituted or metal-free forms[1,10]. Depending on the function or type of porphyrin system, porphyrins have different metal centers and substituents attached at certain sites of the molecule. Naturally, occurring porphyrin structures serve biological importance carrying out function in living systems. Important biological porphyrins are chlorophyll molecules and heme groups in hemoglobin depicted in Figure 2[10]. Through analysis and striving to mimic biological function, research has produced pathways broadening which the scope of synthesis, function and reactions of synthetic porphyrin systems. One of the more studied porphyrins under the class of azaporphyrins are the tetrabenzoazaporphyrins which are known as phthalocyanines[1]. Phthalocyanines are a class of synthetic macrocycle closely resembling porphins, which were accidentally discovered, and documented appearances in reactions were observed dating back as early as 1907 when Braun and Tcherniac at South Metropolitan Gas Company in London synthesized o-cyanobenzamide[2,14]. The structure of the non-substituted phthalocyanine and porphyrin macrocycles can be seen in Figure 1.

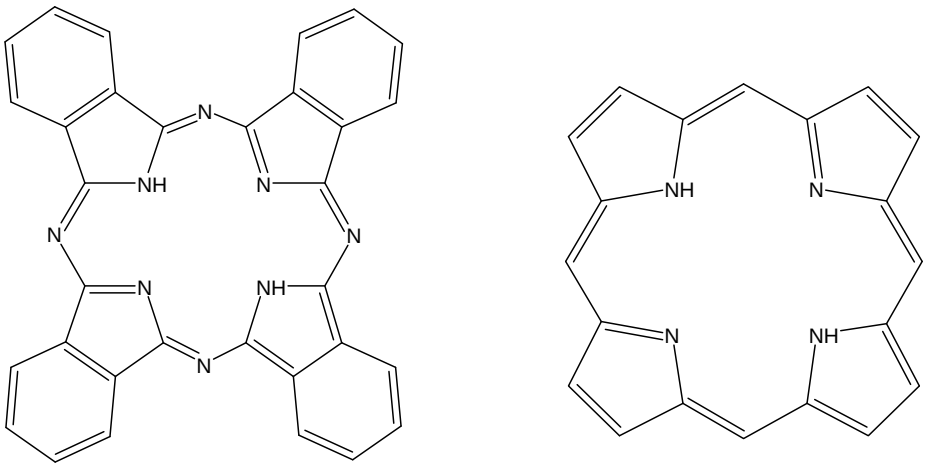

Figure 1. (Left to right) Metal-free phthalocyanine and metal-free porphyrin

Following an attempt to obtain benzonitriles in 1927, de Diesbach and von der Weid synthesized a blue pigmented substance, later confirmed as copper phthalocyanine, which was obtained from the reaction of 1,2-dibromobenzene and copper cyanide. de Diesbach and von der Weid studies into the discovery led to basic properties and chemical formula of copper phthalocyanine[3,14]. After the appearance of what would be classified as iron phthalocyanine in 1928 at Scottish Dyes Ltd. from their preparation of phthalimide, Linstead and his students would continue investigating and classifying the structure of both phthalocyanine and other metal phthalocyanines from 1929 to 1934[4,5,6,7,14].

Applications of phthalocyanines

Upon classification and early studies, phthalocyanines exhibited a pronounced blue-greenish pigment accompanied with resistance to degradation at high temperatures, most solvents and visible light[8,14]. Due to their properties phthalocyanines would become implemented into dyes for their qualities giving distinct colors and stability. Copper phthalocyanine's high fluorescence and simple synthesis was ideal for processes pertaining to pigments and dyes[8,9,14].

Early biological applications pertained to brain tissue stains[8] and investigations were based derivatives of porphyrins, mainly consisting of the hemes and chlorophylls[10]. In Figure 2, Heme b, Heme a, chlorophyll (a or b depending on the R functional group) and metal phthalocyanine are illustrated side by side to show their similar structure, respectively. From comparison, phthalocyanine difference from the parent porphyrin structure are the benzo-moieties at the beta position and aza bridges instead of methine bridges that are discussed in the section titled structure and illustrated in Figure 1.

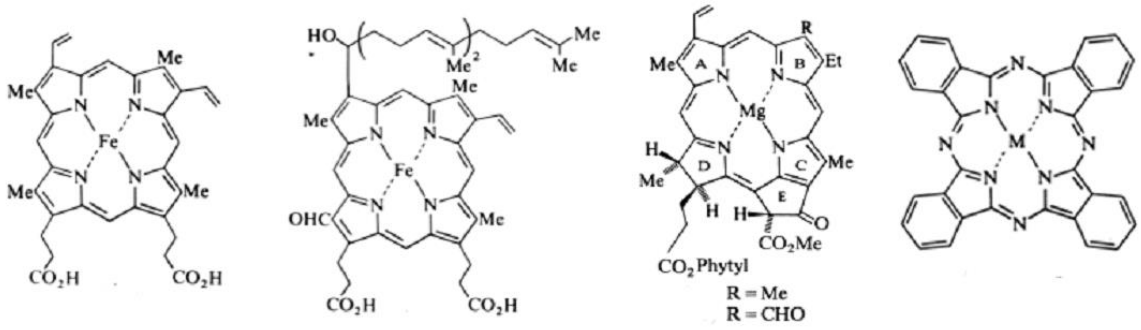

Figure 2. (Left to right) Heme b, Heme a, chlorophyll, a or b depending on R group, and metal phthalocyanine[10]

Adding to their thermal and chemical stability, phthalocyanines are integrated into many optical and electrical devices such as semiconductors, photodiodes, organic photovoltaic cells and photodetectors[11]. Studies of semiconductor properties can be dated as early as 1948[12]. The tunning and optimization of these optoelectronics can be performed by altering the phthalocyanine structure. The attaching of functional groups to the base structure, the choice of metal centers, and the arrangement of layers in films have continued to be studied to refine the desired qualities given by phthalocyanines to optimize the potential devices[13]. Phthalocyanines have been used as catalyst in the oxidation of polychlorinated phenols in the presence of an

oxidizer (hydrogen peroxide) promoting ring cleavage to form different acid products[15]. Catalytic pathways of phthalocyanines holds great interest due to resemblance to other porphyrin systems, which are involved in biological based catalysis; for example, the Heme b group in cytochrome p450 enzymes, attached by an iron-cysteine bond, is active in oxidation processes in mammals, as shown in Figure 3[16].

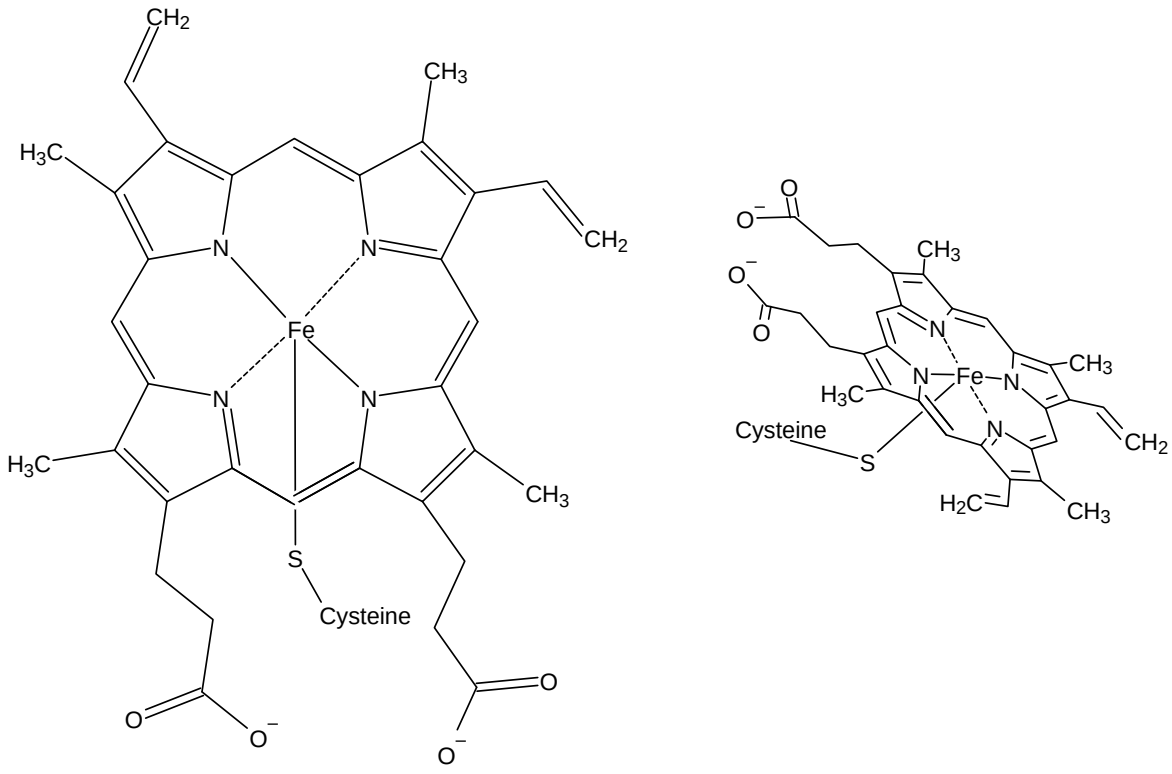

Figure 3. Heme b group in cytochrome p450 enzymes

Levulinic acid

With the inevitable end of fossil fuels in the future, the search for renewable sources of energy has been of great necessity. A possible, abundant source of alternative fuels comes from green chemistry involving hexose sugars from carbohydrates and cellulose. These sugars and cellulose materials originate in biomass sources producing compounds such as levulinic acid. The first synthesis and appearance of levulinic acid was by chemist Mulder heating sucrose with hydrochloric acid believing the product was glucinic acid until later classification[17]. Levulinic acid and its alkyl-substituted alternatives have been shown to be promising precursors for biofuels or as additions to petroleum products from its mention in 2004 U.S. Department of Energy[18,20,21,24]. In addition, the levulinates are highly desired for their reactivity at both substituent sites, the carboxylic acid, ester or ketone, to form other compounds via Fischer esterification, condensations and additions[19,21,22,24]. These compounds have a diverse range of applications in areas such as pharmaceuticals, preservatives, plastics and the synthesis of γ-valerolatone, which has been regarded to be the desired conversion product for the production of liquid fuels and chemicals[18,19,22]. Figure 4 shows the possible products and uses from the conversions of levulinic acid. Upon later identification of levulinic acid from sugar cane in the 1870s using inorganic acids[26,27] and continued changes in synthesis thru the 19th century[28], the reactions had drawbacks which included: high-cost margins, low yields, high temperatures/pressures, excessive purification, too many steps and low environmental-friendly outcomes[19,20,24]. At the turn of the century, interest in refining the synthesis of levulinic acid evolved many innovative methods using different catalyst systems[20], solvent mediums[23,24,32,33], one-pot syntheses[24], eco-friendly methods[24], etc. The drive behind the synthesis for innovation

would be to make the synthesis of levulinates feasible to produce bulk at an industrial scale reducing cost and making compounds readily available and increase research opportunities.

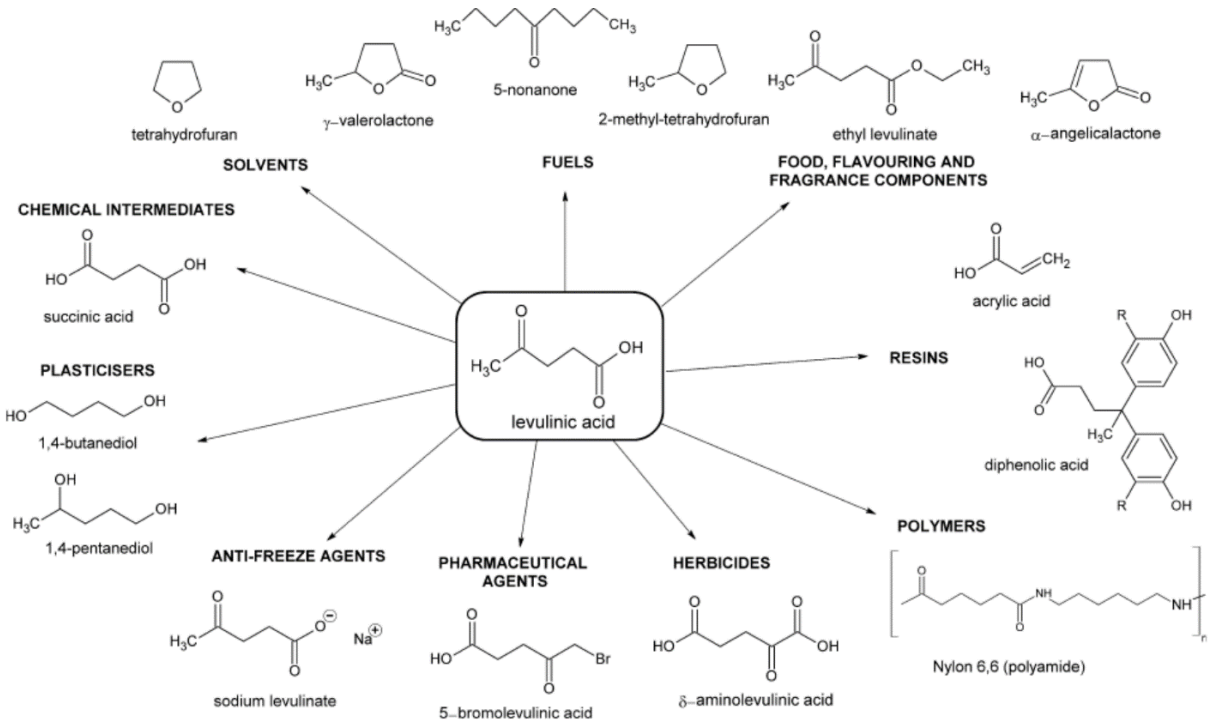

Figure 4. A flow chart of possible derivates of levulinic acid[19]

CHAPTER II

INTRODUCTION

Structures, properties and geometries of porphyrin systems

As stated previously, phthalocyanines originated as a byproduct from synthesis aiming to derive another product. Their basic structure resembles that of the parent's chemical design labeled as porphyrins. Being derivates of naturally occurring porphyrins, phthalocyanines are more closely related in macrocycle layout with that of another synthetic porphyrin system called tetraazaporphyrin or its more common name porphyrazine. Figure 5 and 6 illustrates the resembles and alterations to the skeletons from the parent to phthalocyanine with the porphyrazine as an intermediate analog.

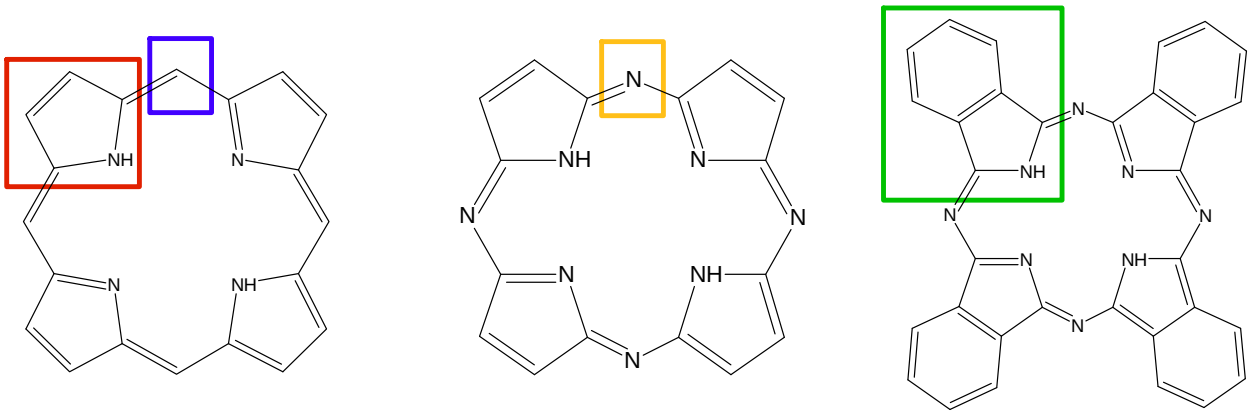

Figure 5. Similar structures for metal-free porphyrins, porphyrazines and phthalocyanines respectively

As shown on Figure 5 and 6 the structure and size of the macrocycle diversifies from porphine, free base porphyrin, to metal-free phthalocyanine with unsubstituted porphyrazine in the middle. Key differentiations would be the replacement of methine bridges (blue box) on the meso position of porphyrins with aza bridges (orange box) for both porphyrazines and phthalocyanines. Another alteration would be the addition of benzene rings on the β-positions (blue Greek letters) of the porphyrins and porphyrazines yielding the phthalocyanine structure. The interpretation of the subunits making up the phthalocyanine skeleton can be viewed in two representations. Referring to the porphyrin structure, the nucleus of phthalocyanines are porphyrazines with benzene rings on the β-positions consisting of four pyrrole subunits (red box). The other way would be phthalocyanines consist of four isoindole subunits (green box) fused together by aza bridges making up the macrocycle[10,14,40]. In either case, two central nitrogen atoms containing protons would be classified as iminos while the other two central nitrogen atoms would be categorized as imines due to the nitrogen-carbon double bond.

Porphyrins and porphyrazines have 11 π bonds while phthalocyanines have 19. The highly conjugated macrocycles have π bonds that contribute to two possible resonance structures that could be seen from Figure 6 depicting the delocalized electrons across the bonds associated with them.

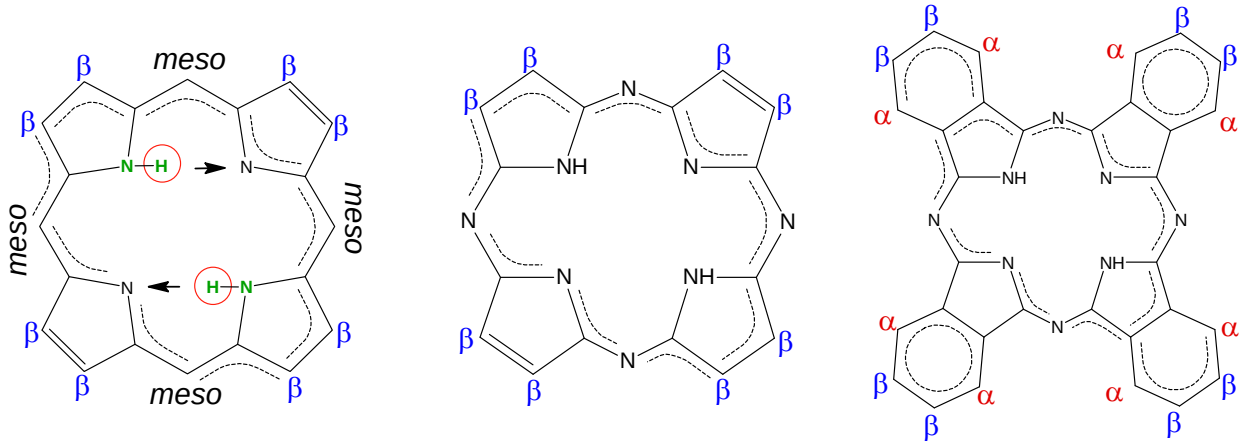

Figure 6. Positions of possible alterations to macrocycles and delocalization of conjugated π bonds

Every molecule at its core has 9 π bonds involved in resonance but, fundamentally, they have 22 π electrons participating in resonance with the lone pair on sp2 nitrogen atoms containing protons in the center labeled in green in Figure 6. It is due to a p-orbital correlated with sp2 nitrogen having the lone pair electrons out-of-plane and perpendicular to the molecule. The sp2 nitrogen have the corresponding p-orbitals give π bonds associated with the entire macrocycle making them parallel to each other. Figure 7 depicts the possible molecular orbitals, p-orbital orientations and electron interactions giving a visual representation related to the porphyrin derivatives[41].

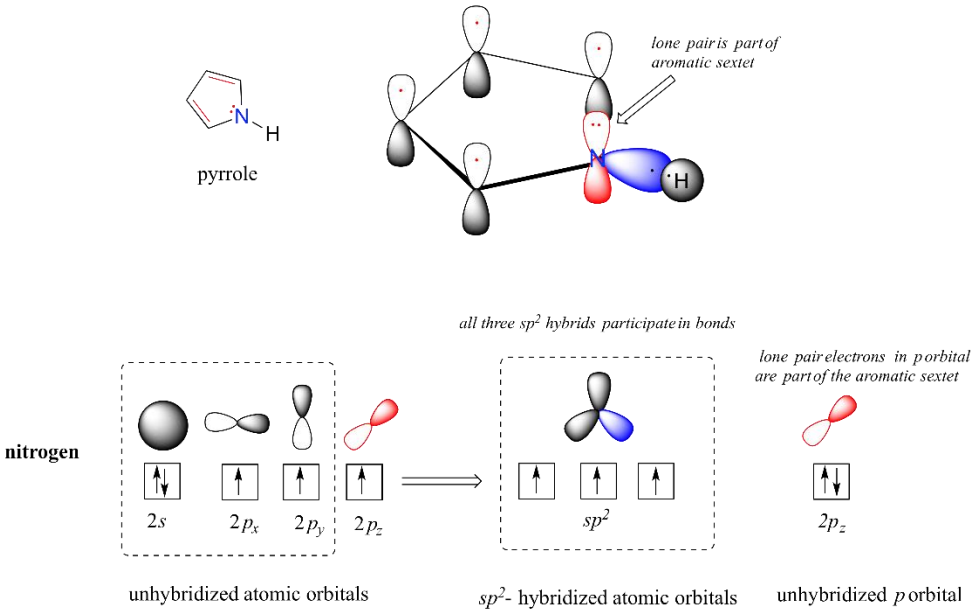

Figure 7. Molecular orbital layout for pyrrole[41]

The resonance is subject to change for reasons pertaining to a proton transfer, illustrated in Figure 6 by the red circle, the emergence of a cation due to proton addition or deprotonation which could result in the dianion achieving desired condition for metalation. The only exception would be the phthalocyanine structure where the benzene rings having their own resonance or are part of the resonance taking place within the core of the molecule.

Homogenous porphyrin systems tend to have high symmetry, which aids their characteristic high stability, aromatic molecules obeying Hückel's rule[10]. Homogenous, unsubstituted porphyrins and analogs have D_{4h} symmetry, which designates a central C_4 axis perpendicular to the square planar geometry of the molecule (out-of-plane), four C_2 axis perpendicular to the central axis (in-plane) and a σ_h mirror plane perpendicular to the central axis[40]. Figure 8 shows the axes and σ_h mirror plane (green lines) related to the point group of D_{4h} symmetry with color coordination to distinguish the C_4 axis (red) from the C_2 axes (blue).

Heterogenous porphyrins and some analogs have low symmetry due to alterations to the outer portions of the macrocycle. For porphyrins, lower symmetry would be due to substituents attached at the meso and β positions on the molecule. For phthalocyanines, reduced symmetry occurs when substituents are added to the α (red Greek letters) and β positions. The reduction of symmetry, the point groups would be restructured to meet the new symmetry elements with either the rotational group or mirror planes. For example, if a porphyrin system were heterogenous due to different substituents on meso or β positions, C_2 axes would be reduced and a loss of the σ_h plane would occur due to non-matching folds. Lower symmetry point groups would be generated starting with the D_{2h} point group to minimal symmetry systems containing only the C_s point group would be possible. Some of the reasons for achieving lower symmetry on these macrocycles would be to alter properties such as, increase reactivity and solubility to implement, which makes the molecule more useable for electronic devices. In addition, due to the alterations to the peripheral areas of the porphyrin macrocycles the conjugated π system becomes disrupted[43,44].

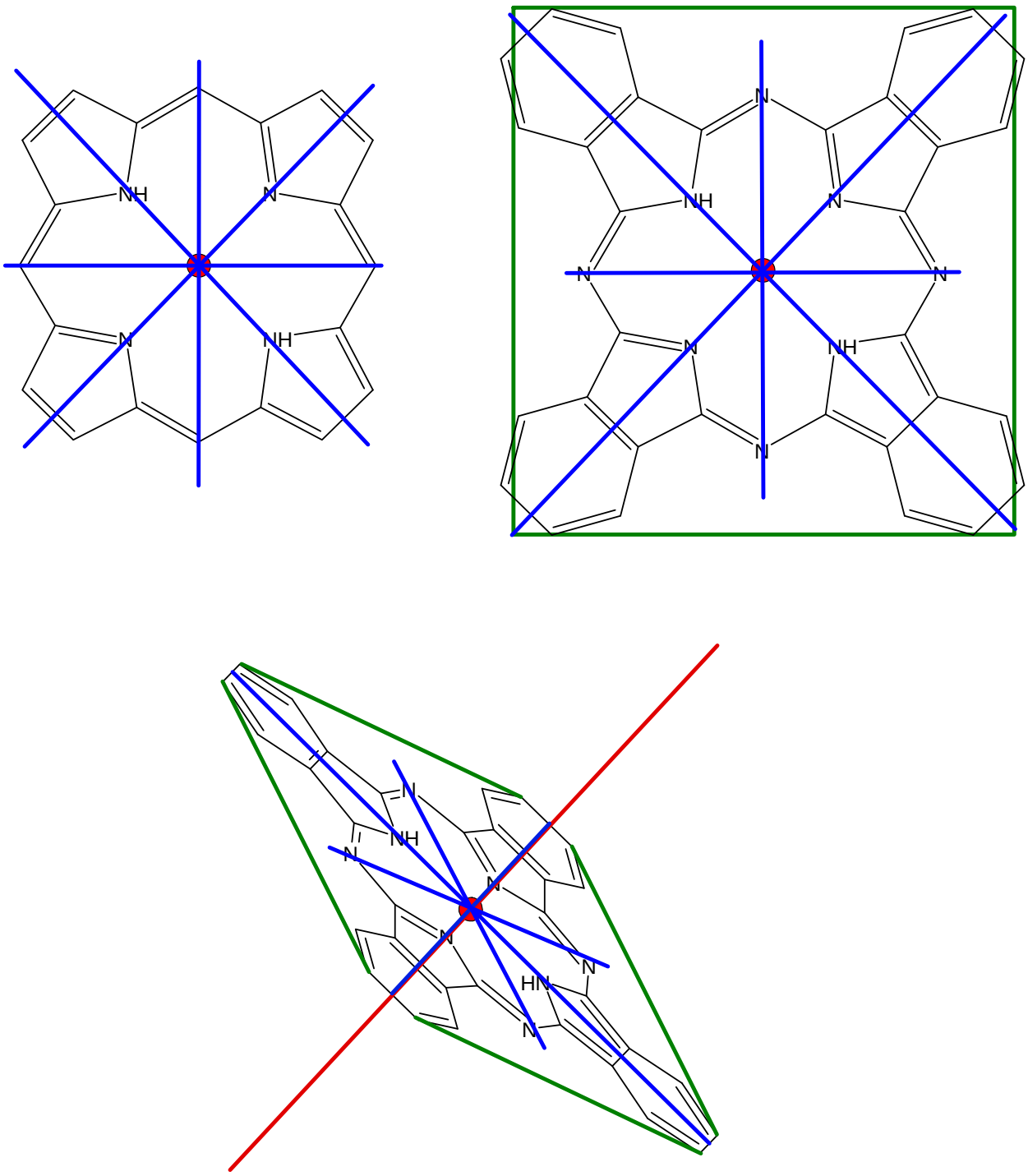

Figure 8. Axis and plane of porphyrin and phthalocyanine

The complexity, reactivity, and properties of porphyrin systems tend to change after metalation, which allows for the addition of different metal centers. As previously stated, metal-free porphyrins and analogues that are flat, two-dimensional, square planar geometries that attribute to their high stability. Once metalation is achieved and depending on the oxidation state of the metal center, the geometry of the macrocycle system would conform to the interactions with the metal, which could possibly occur from axial ligand additions or formation of higher complex molecules with the stacking of monomer structures.

For porphyrins and phthalocyanines, one method for addition of the metal to the center begins with deprotonation of the ring structure creating a tetradentate center coordinating a metal ion to the four nitrogen atoms. Metal ions with different ionic radii can bind to the tetradentate center satisfying the parameters and stabilizing the macrocycles. The parameters for each structure have been studied using x-ray techniques in literature[40,45]. For metal-free porphyrins, each nitrogen atom is between 406-420 pm from neighboring nitrogen atoms diagonally and 291-292 pm laterally from nitrogen neighboring atoms. The distance for each nitrogen to the center of the molecule is between 203-210 pm. These distances can almost fit any metal ion within the core. The metal-free phthalocyanines, the parameters are close to those of porphyrin with the values of the central nitrogen from each other ranging 365-450 pm diagonally, 260-285 pm laterally and 182-225 pm for each central nitrogen from the center of the core.

Upon the formation of the dianion from deprotonation of the porphyrin or phthalocyanine center, cation metal ions having different oxidation states can fill the negatively charged gap. An ideal metal center would be a metal tending to remain a divalent cation to conserve the geometry for the system. Although some metals can stay divalent such as alkali earth metals, typically

metal ions interact with their surroundings resulting in either oxidation or reduction. From these possibilities, the addition of ligands to the metal center have been shown to occur or the development of polymers forming higher coordination complexes with different geometries from the square planar of metal-free porphyrins and analogs. Figures 9 and 10 illustrate the position and effects of possible ligands on the axial positions of metal porphyrin structures having higher than divalent oxidation states[42]. Figure 11 shows the possible phthalocyanine geometries are shown from monovalent, divalent, trivalent, tetravalent and pentavalent metal centers[40].

Figure 9 shows the porphyrin following the metalation process using a divalent metal ion with two alternative pathways incorporating axial ligands with further oxidation of the metal center or the metal center at a tetravalent state. The six coordinated complex has ligands bonded on the same side giving the cis conformation of the structure or on opposite sides giving the trans conformation. Visually, cis conformation would yield a cross between tetrahedral and seesaw molecular geometry with ligands possibly having a pull effect on the metal center shifting out-of-plane. While trans conformation, the structure takes on a more octahedral geometry.

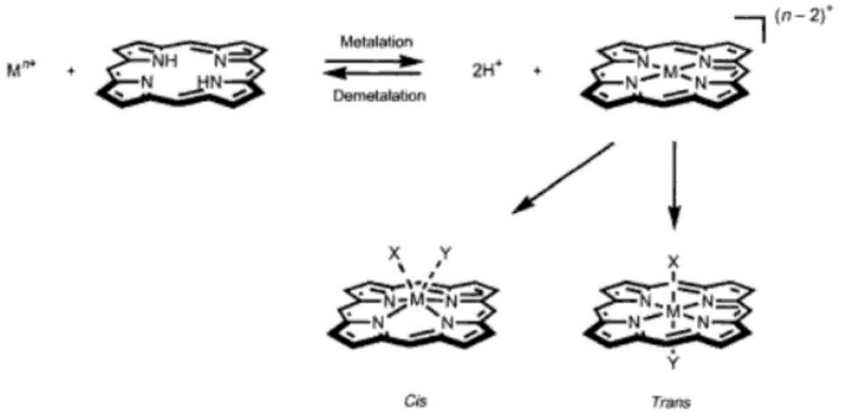

Figure 9. Metalation of porphyrin with axial ligand interactions[42]

In Figure 10, an equilibrium scheme shows different ligands binding to the metal porphyrin center via two methods. The first method with two equilibrium constantans, K_1 and K_2, exhibits interchangeable ligands with none, one or two binding to the metal center, labeled with M, having reversable capabilities. These ligands labeled with a L have a weak binding and depend on the stability of the complex. The second method with one equilibrium constant, K, displays one ligand bonded constantly with another being interchangeable. The ligand fixed to the core is labeled with a X having a strong bond.

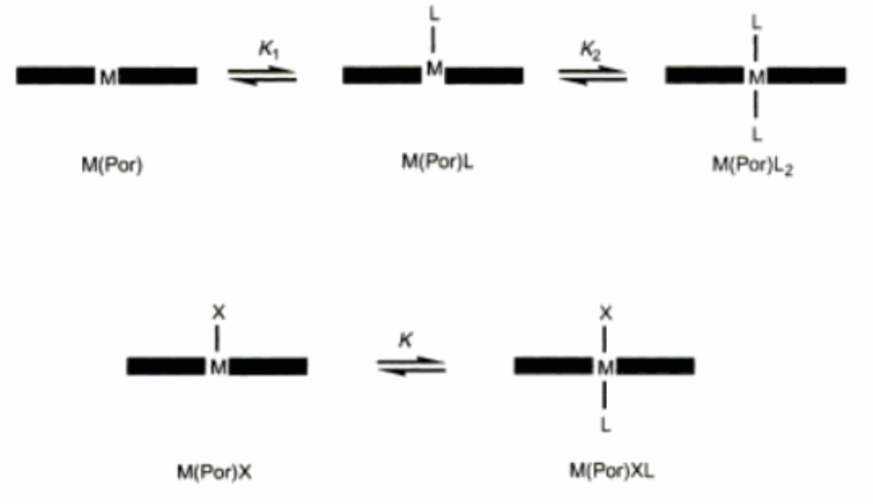

Figure 10. Possible ligands at the axial position for metal porphyrins: M = metal center, L = exchangeable ligand, X = fixed ligand[42]

Figure 11 shows phthalocyanine metal complexes with different geometries, which are related to the oxidation state of the metal center starting from monovalent, ions, to the pentavalent ions. Depending on the ionic radii, oxidation state, nature of the metal, molecular geometries have shown different ligand additions, metal-metal interactions, and formation of polymers resulting from porphyrin complexes, with the phthalocyanines being tetradentate

dianions in their reduced state from deprotonation. Since porphyrins and phthalocyanines have similar chemical aspects, Figures 9, 10 and 11 are related molecular geometries, which are not limited to either species. New complex geometries have shown metal centers out-of-plane due to metal ion size being large, a metal center bridging two phthalocyanines, two metal centers bound to a single phthalocyanine, metal-metal interactions bringing two phthalocyanine complexes, and the stacking of multiple phthalocyanines with different metals out-of-plane. Except for the two metal centers bound to one phthalocyanine due to a monovalent state, all other molecular geometries would be possible with metals exhibiting divalent or higher oxidation states. As for a divalent out-of-plane metal center geometry, the ionic metal radii would be large promoting the associated geometry and can be assigned to atoms such as lead and platinum.

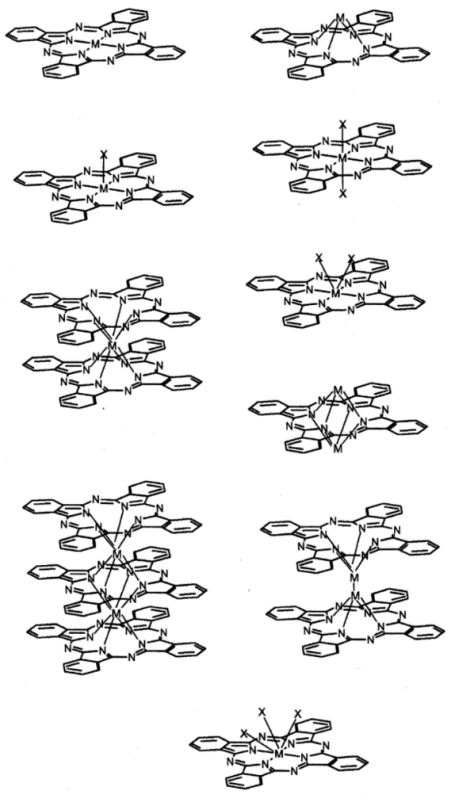

Figure 11. Possible molecular geometries for phthalocyanines with different metal ions[40]

Understanding the possible molecular geometries of porphyrin-like structures with or without a metal center, alterations to the homogenous structure of a porphyrin or phthalocyanine disrupts the conjugated π system, allowing for properties to change allows for their use in different areas of electronics, catalysis and optoelectronics[13,15,43,44]. Results of these distortions promoting optimization of these macrocycles are expressed as Soret bands having a red shift, Q bands increasing, lower symmetry and reduction of molecular geometries[44,46]. Another area for exploration to understand the changes in properties associated with geometries has been crystal field theory of the metalloporphyrin complexes and splitting of molecular orbitals of the metal with interactions of all ligands. These studies would include axial ligands, other ligands attached to the metal center, the porphyrin or phthalocyanine structure since the ring becomes a tetradentate ligand upon deprotonation of the imino groups.

Synthesis of phthalocyanines

As stated earlier, phthalocyanines are classified as synthetic molecules, as they do not naturally occur in nature, unlike the parent porphyrin structure. With synthetic approaches, homogenous and heterogenous phthalocyanines can be created using readily available precursors. For the homogenous class of phthalocyanines, Figure 12 shows the possible starting precursors where the four units combine via condensation reactions to make the framework of the macrocycle. Whereas Figure 13 outlines reactions involving the precursors of choice with the addition of mostly halogenated metal complexes. The addition of the metal causes the metal substituted phthalocyanine synthesis and possible metal-ligand attachments. Figure 13 shows how a divalent metal halide attaches, which most resembles group two of the periodic table. The

divalent metal ion reacts with a precursor shown in Figure 12 and yields a metal phthalocyanine without any axial ligands attaching to the metal center of the molecule[36,43].

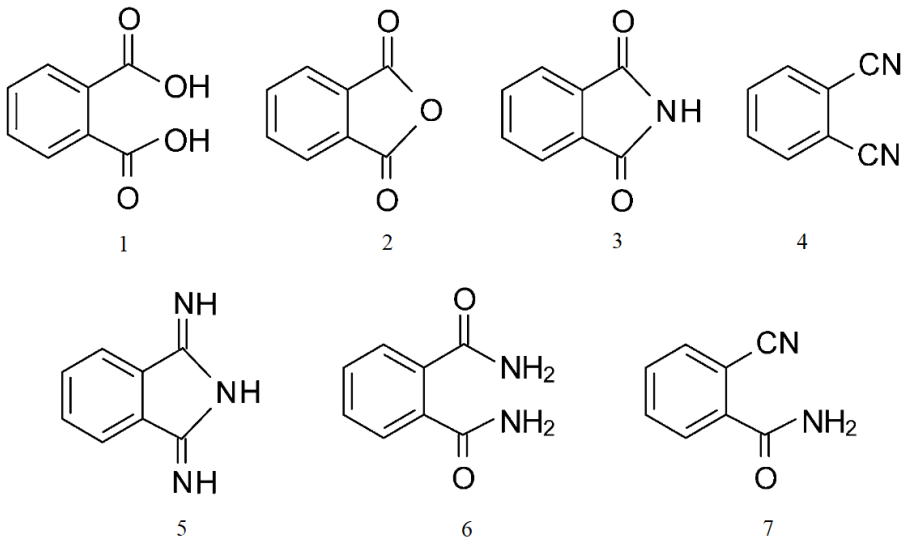

Firgue 12. Precursors to form phthalocyanines: 1) phthalic acids, 2) phthalic anhydrides, 3) phthalimides, 4) phthalonitriles, 5) 1,3-diiminoisoindolines, 6) phthalamides and 7) 1-benzamidecarbonitrile[36]

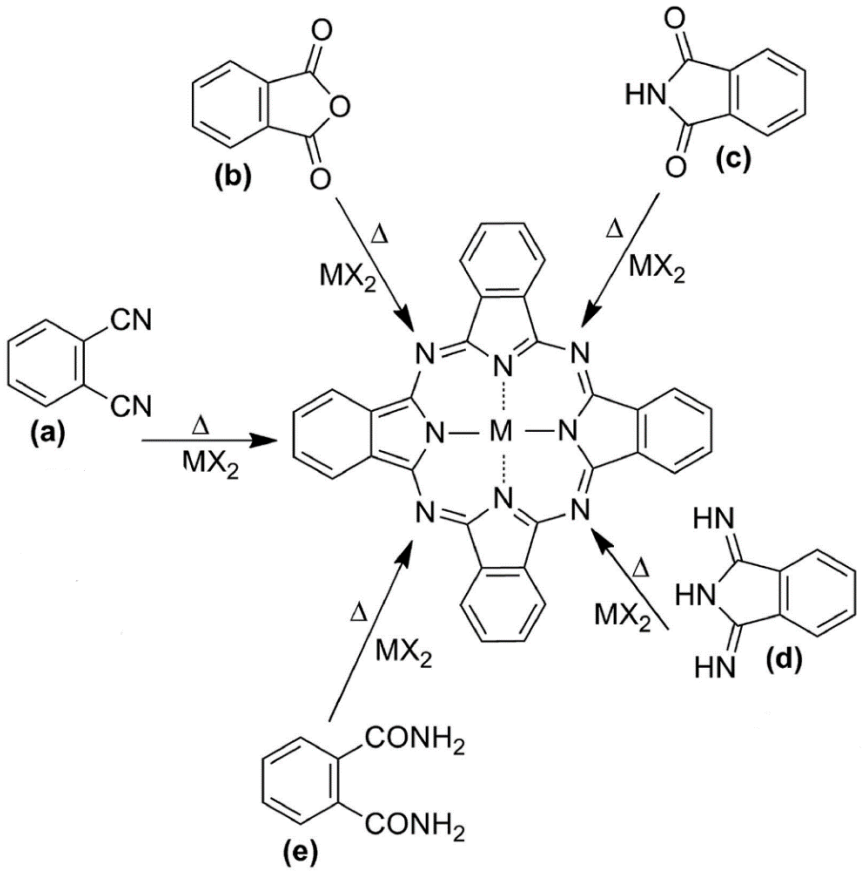

Figure 13. Outline of precursors interacting with metal halides to form metallophthalocyanines: a) pthalonitriles, b) phthalic anhydrides, c) phthalimides, d) 1,3-diiminoisoindolines, e) phthalamides[43]

For heterogenous phthalocyanines, modifications to the non-peripheral α and peripheral β positions of the phthalocyanine ring can occur thorugh two methods. The first method would be the use of precursors modified with the desired substituents producing heterogenous phthalocyanines tailered for their intended use. The second method involves postsynthetic modification of the phtalocyanine molecule using different processes to attach substituents directly to the peripheral or non-peripheral positions of the synthsized macrocycle[36]. The best approach gernerally is accepted to be the first method to obtain consistent complexes since

substituents are directed to their preferred positions. The second method typically generates a mixture of products, which are difficult to identify and separate the similar structures. Using either method, the heterogenous pthalocyanines have low symmetry, higher reactivty and their increased solubility makes them canadiates for catalysis or electronics due to the effects the substituents have on the stability of the pthalocyanine complexes. The properties are dependent on the substituents; if the subsitutents are either electron donating or electon withdrawing groups, the absorption range of the pthalocyanine complexes can be made greater in the visible region for electron donating groups with electrons neighboring the conjugated π system of the complex such as esters or alcohols. As for electron withdrawing groups such as sulfonates or nitrites, the stability, solubility and ability to attach the pthalocyanine structure to other molecule surfaces would be affected making their application different from homogenous pthalocyanines[36]. The position of the groups on the outer ring changes the absorption spectra whether on α or β along with the disruption of the other attributes of phthalocyanine complexes[47].

Vanadium phthalocyanine

Vanadium was first discovered and labeled a new element in 1801 by a professor of mineralogy, Andres Manuel del Rio, in Mexico City until he later reverted his discovery thinking it was another form of chromium. In 1831, a Swedish chemist, Nils G. Sefström, confirmed the new element discovery and named it after the Scandinavian goddess, Vanadis. The transition metal is common in most mineral and fossil fuel deposits with its average abundance being roughly 150 parts per million. In mining for magnetite ores, magmatic ores, oil, minerals or uranium, vanadium metal deposits are rare on their own and exist in many different compounds such as vanadium pentoxide[48,49]. Vanadium pentoxide is a commercially important catalytic

compound used in modern sulfuric acid production. Different mechanistic and kinetic studies have shown vanadium oxides exhibit catalytic properties in oxidation reactions[49]. The catalytic activity of vanadium is expressed in nature as vanadium is incorporated into the active sites of a class of haloperoxidase enzyme, vanadium bromoperoxidase, found in marine algae that brominate hydrocarbons due to removal of produced hydrogen peroxide associated with photosynthesis[50]. In addition, vanadium replaces molybdenum/iron in nitrogen-fixing bacteria nitrogenases to form vanadium nitrogenase[51,52]. Figure 14 shows the structures of the active sites in each enzyme respectively.

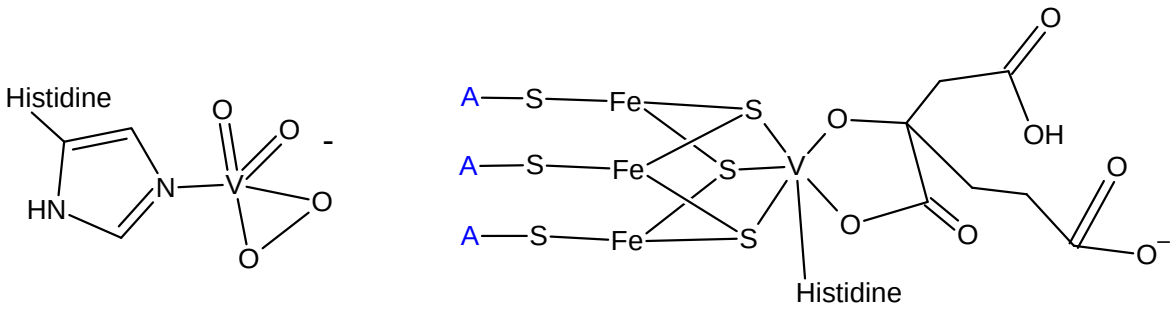

Figure 14. Structures of vanadium active sites of vanadium bromoperoxidase and nitrogenase (A – Any atom)

Research in catalytic activity of vanadium phthalocyanine has not been explored extensively. Due to the air sensitivity and strong tendency to oxidize, vanadium phthalocyanine shows an oxovanadium center, with a tetravalent center. Eguchi et al. studies showed the synthesis of a divalent vanadium center being achieved using ultra-high-vacuum conditions[11]. Figure 15 shows the two metal centers for oxovanadium (V^{4+}) and vanadium (II) phthalocyanine.

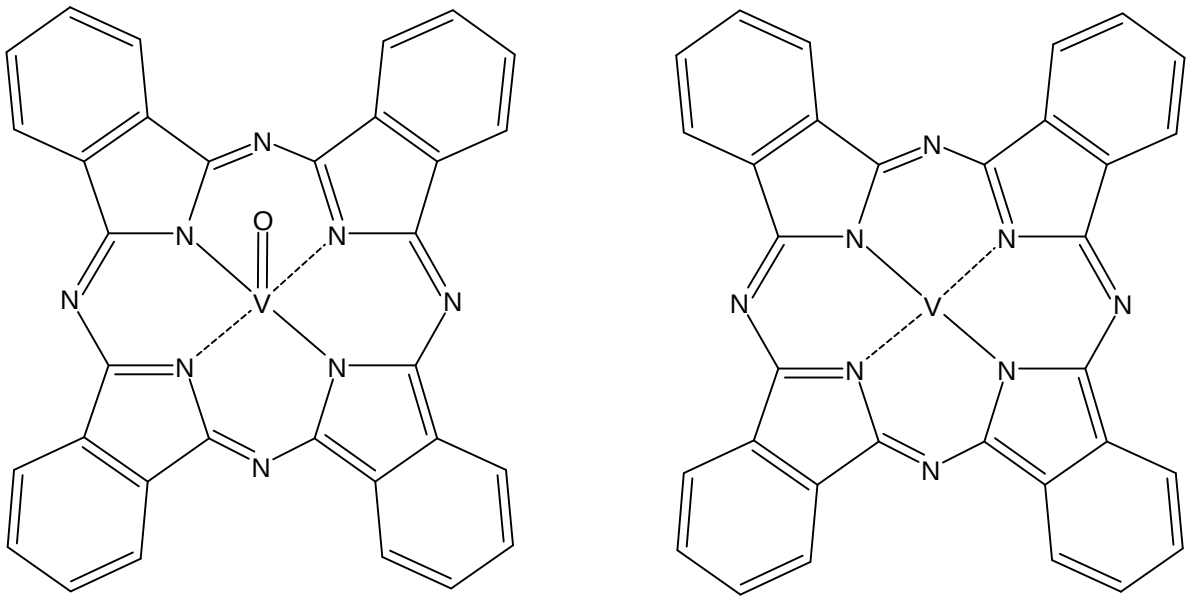

Figure 15. Structures for oxovanadium (V^{4+}) and vanadium (II) phthalocyanine

Catalytic pathways of metallophthalocyanines

Metal phthalocyanines have been shown to be usable catalysts in redox reactions. Their importance in redox reaction has arose from exploration of phthalocyanines with or without substituents exhibiting oxidative properties on hazardous environmental chemicals. Studies used different metallophthalocyanines in combination with an oxidizer to oxidize halogenated phenols which aided in ring cleaved products[15]. Iron, manganese, cobalt, and nickel metal centers associated in the metal tetrasulfophthalocyanine centers. The study with an iron tetrasulfophthalocyanine/hydrogen peroxide combination showing high promise as a phenol oxidizer. The catalyst of choice can be seen on Figure 16. A notable quality of the chemical structure was increased solubility due to the sulfonate substituent on the peripheral positions of the phthalocyanine complex allowing for easier extraction upon conclusion of the study.

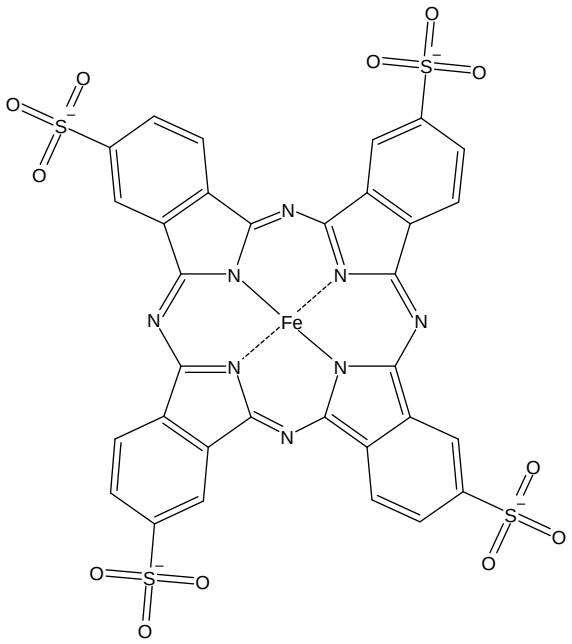

Figure 16. A water-soluble catalyst, iron tetrasulfophthalocyanine

Data suggests the elimination of halogen substituents via the catalyst/oxidizer combination and arrival at the final oxidized products were influenced by an iron (III) peroxo complex from the interactions of the favored combination. Figure 17 illustrates a simplified reaction for the study.

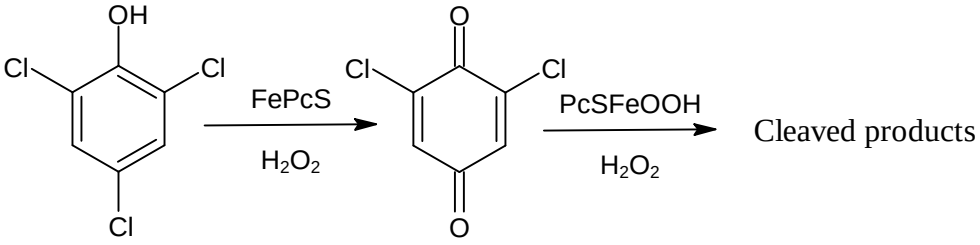

Figure 17. Catalytic reactions oxidizing chlorinated phenols

Adding to the oxidations of pollutants, the same combination was studied in oxidation of starch molecules in later studies following the oxidation of halogenated phenols[37]. Figure 18

exhibits the purposed mechanism of the oxidation of starch molecules. Changes to previous oxidation methods of starch were performed to optimize desired outcomes and eliminate the production of unnecessary inorganic waste. The initial iron catalyst, iron (II) sulfate, was replaced with the iron tetrasulfonatophthalocyanine to allow oxidation to occur on the surface of the starch molecules in the study while eliminating the production of waste. The iron sulfate catalyst was shown to be small enough of an ion to enter and react with starch molecules. The iron phthalocyanine choice was a large macrocycle allowing for the activation of the catalyst/oxidizer combination via the surface without the formation of iron/starch complexes. Starch was treated with ultrasound transmitters for 24 hours to view the effect of sonification had on the method.

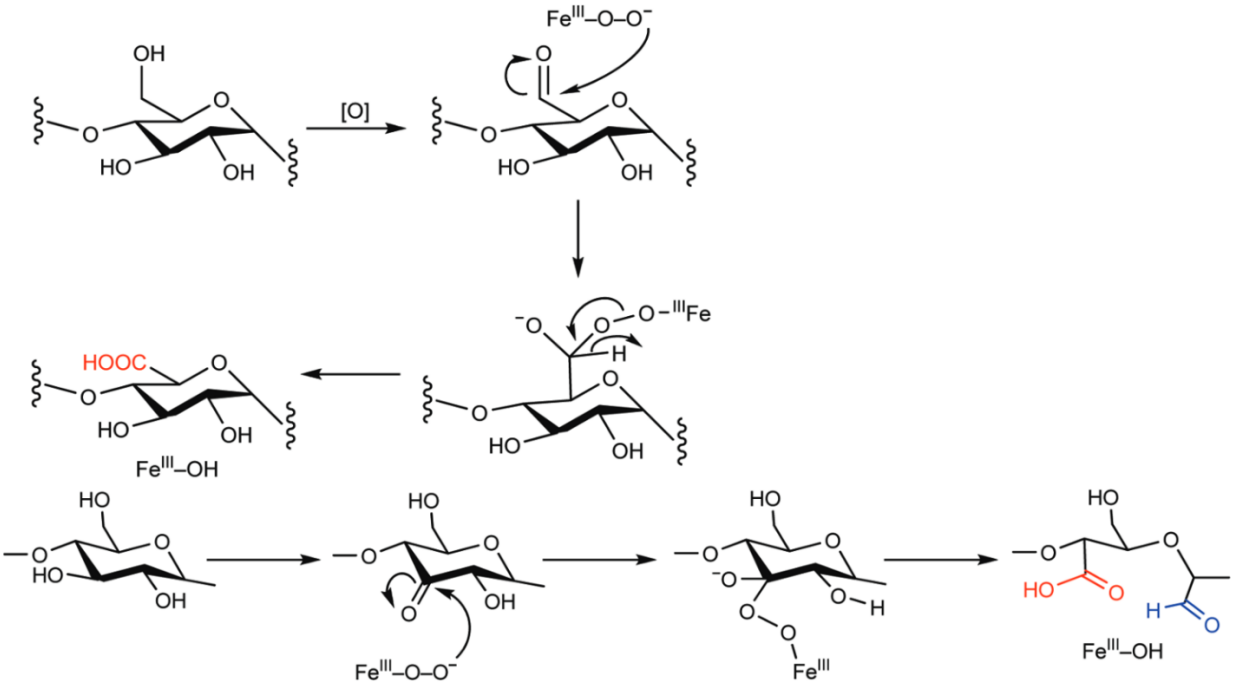

Figure 18. Purposed mechanism for the oxidation of starch molecules reacting with an iron catalyst/hydrogen peroxide combination[37]

Recently, studies have been performed exploring the catalytic properties of unsubstituted metallophthalocyanine combined with hydrogen peroxide as an oxidizer in removing endocrine disrupting compounds[38]. Results showed both manganese and iron phthalocyanine were good catalysts in the removal of the targeted compounds. Adjustments of the concentrations of hydrogen peroxide and addition of acetonitrile influenced the reactions at different pH's. Iron phthalocyanine was shown to be productive in neutral conditions outperforming optimal removal of desired compounds by manganese phthalocyanine under acidic conditions. Table 1 summarizes the optimal catalytic conditions for Mn and Fe phthalocyanine compounds on the removal of endocrine disrupting compounds. The catalytic properties of phthalocyanines have been validated in different studies over the years along with the results showcased in this study.

Catalyst	H_2O_2	No H_2O_2	Acetonitrile	No acetonitrile	pH 3	pH 7
MnPc	✔	✘	✘	✔	✔	✘
FePc	✔	✘	✔	✘	✘	✔

Table 1. Optimal conditions for each phthalocyanine.

MnPc = manganese phthalocyanine, FePc = iron phthalocyanine

Syntheses of levulinates

Different types of biomass materials have been explored and referenced through the years trying to synthesize levulinic acid effectively. The common factor in all the synthesis is a breakdown of the biomass source to simple hexose sugars, monosaccharides with six carbon atoms, via heated, acid-catalyzed reactions in aqueous medium using inorganic acids such

sulfuric and hydrochloric acid illustrated in Figure 19.Studies have altered aspects of the synthesis to monitor the effects certain acid concentrations, pressures, solvent mediums, starting points or temperature parameters have an influence on the effectiveness of the reaction[18,20,23,24,25,29,32,33]. Ideal reaction changes would be those making biomass degradation feasible and exhibiting high yields of levulinic acid.

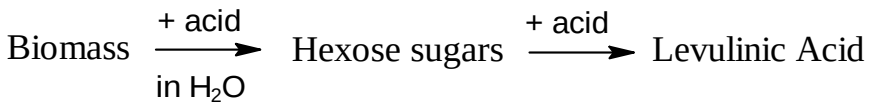

Figure 19. Simplified reactions for synthesis of levulinic acid from biomass

The source of biomass can control the composition of polysaccharides such as cellulose or starch. Cellulose would come from the structural framework components containing β-D-glucose molecule chains and starch comes from the energy storage aspect made up of either amylose or amylopectin chains. The sugar extracted from the decomposition of cellulose and starch molecules would be glucose. Another carbohydrate, from biomass such as sugar cane, named sucrose can be acquired being the transport protein in some plants. The sugars extracted from breaking down the disaccharide would be a mixture of glucose and fructose in equal proportions. Once the hexose sugars have been derived and due to extractions happening in acidic conditions, the synthesis can take two mechanisms of action. One mechanism involves a keto-enol tautomerization converting some aldose molecules to ketose molecules by shifting protons on carbon 1 and carbon 2. The other mechanism forms an intermediate enediol resulting from transformations of both the glucose and fructose molecules. After the tautomerization or

formation of the intermediate a dehydration follows making the 5-hydroxymethyl furfural (HMF). After HMF undergoes a rehydration resulting in the desired product of levulinic acid plus formic acid. The difference in mechanism would be the tautomerization mechanism follows a cyclic route to form HMF while the intermediate mechanism follows an acyclic route. Scientific evidence favors the fructose and the cyclic route. The mechanistic details are following literature and simplified in Figure 20[19,29,30,31].

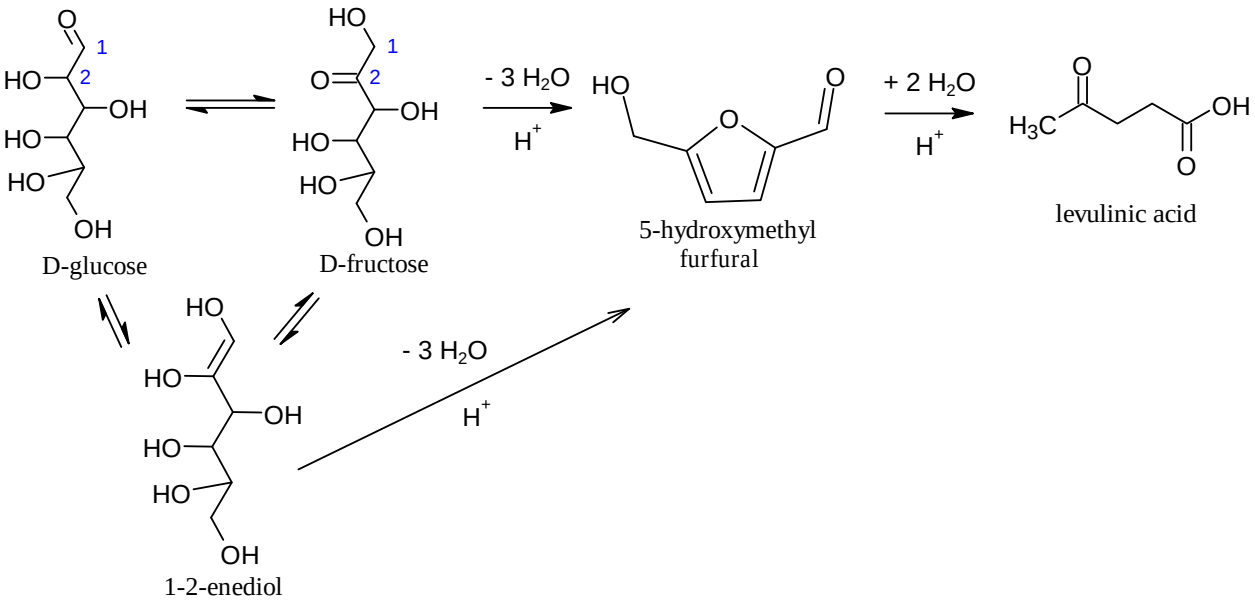

Figure 20. Mechanism leading to the formation of levulinic acid

Other levulinates can be achieved by esterification of levulinic acid in an acid-catalyzed reaction with an alcohol as seen in the literature[34]. Recently, the approach to obtain these alkyl levulinates has been refined by altering different synthesis methodologies and beginning the reaction from a biomass source rather than a hexose sugar which proves to be crucial to utilize resources[21,35]. The alternative conditions would consist of choices in catalyst, solvent (alcohol substrate) and starting source of sugar with different ratios, conditions or time

durations[20,23,24,32,33]. Overall, the reactions would have similar mechanism attributes with those pertaining to the synthesis of levulinic acid as illustrated in Figure 21.

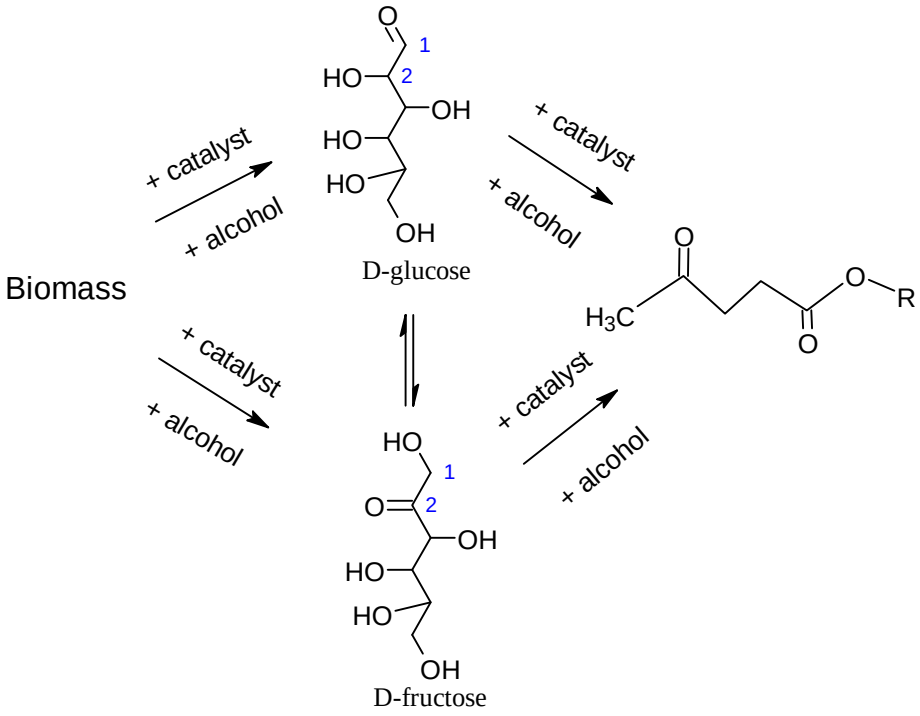

Figure 21. Mechanism leading to the formation of alkyl levulinates

CHAPTER III

MATERIALS AND METHODS

Materials

All reagents were provided by the University of Texas at Rio Grande Valley laboratory facilities at the Brownsville campus and of reagent grade for all experiments. All glassware, synthesis setups, instrumentations and gases originated from the UTRGV.

Synthesis of vanadium phthalocyanine

The synthesis of the vanadium substituted phthalocyanine was achieved following a modified version of the method from Weber and Busch[39]. In brief, the synthesis was performed using microscale quantities, which were as follows: 0.081 mol of phthalic anhydride, 0.045 mol of ammonium chloride, 0.485 mol of urea, 0.0003 mol of ammonium molybdate and 0.024 mol of vanadium (III) chloride and the mixture was ground to a fine powder using a mortar and pestle. After grinding the mixture, the powder was added to 40 mL of nitrobenzene. The mixture was under an inert atmosphere and a Schlenk line was used to supply nitrogen gas. In addition, the reaction was performed using continuous stirring at 180°C and the temperature was controlled using a type K thermocouple synced to a heating mantel for six hours. After six hours, a blueish precipitate formed indicating the synthesis of the vanadium substituted phthalocyanine. The reaction mixture was cooled to room temperature, the product was collected using vacuum

filtration while washed using methanol until the odor of nitrobenzene was gone and all visible impurities had been removed. The purified phthalocyanine product was classified as the vanadyl (IV) phthalocyanine, shown in Figure 15.

FT-IR analysis of vanadium phthalocyanine

The synthesized vanadium phthalocyanine was characterized using a PerkinElmer Frontier FT-IR spectrometer. The vanadium phthalocyanine IR spectrum was compared to the unsubstituted phthalocyanine complex and a purchased standard vanadium phthalocyanine. The data was collected in attenuated total reflectance (ATR) mode, in absorbance units (A) with scans from 4000 to 650 wavenumbers (cm^{-1}), with a 2 cm^{-1} resolution. A mid-IR source was used with a potassium bromide beam splitter to a sample disk, with an ATR consisting of a zinc selenide crystal, and a lithium tantalate detector. At the sample site, a pressure arm attached to a (ATR) attachment which applied 90 newtons of pressure to press the sample against the crystal surface for data collection.

X-ray diffraction patterns of vanadium phthalocyanine

The vanadium phthalocyanine was characterized using X-ray powder diffraction (XRD). A Bruker D2 Phaser XRD was used to collect the data for the substituted and unsubstituted phthalocyanine complex data. The diffractometer operating conditions were as follows: cobalt x-ray source emitting at 1.789 Å (Co K_α), an iron filter, a step of 0.05° with a 2s counting time, a data range from 5 to 50 in 2θ. The XRD data was fitted using the Le Bail Fitting procedure in the Fullprof software and crystallographic data from the literature[53,54,55,56,57,58].

Catalytic reactions of fructose using vanadium phthalocyanine

The reactions of fructose were performed in acidified methanol under reflux conditions using an inert atmosphere. The reactions were performed as follows: a three-neck 125 ml round bottom flask with a 1:9 mmol ratio of vanadyl (IV) phthalocyanine to D-fructose and methanol (40 mL). One milliliter of the acid to be tested was added, which were either hydrochloric, sulfuric, nitric or hydrobromic acid was added. The degassing procedure consisted of alternating vacuum and N_2 gas purges to remove O_2 flowed by a constant pressure of N_2 gas over the reaction mixture. The start of the reaction was considered when the mixture reached reflux temperature, at which point a sample was withdrawn as the zero point of the reaction (T=0). The monitoring the reaction was performed over 24 h time-period. All samples were analyzed using gas chromatography-mass spectroscopy.

Gas chromatography/Mass spectroscopy analysis of reflux reactions

All reaction samples analyzed using a PerkinElmer gas chromatographer with a TurboMass Gold mass spectrometer (GC-MS) for concentration and product identity. The GC-MS was operated using the following conditions: a 1 μL injection, injector temperature of 260° C, helium carrier gas at a pressure of 10 psi, and a diphenyl column. The oven temperature ramp was 25° C to 250° C at a rate of 25° C/min with a hold time of two minutes at the final temperature. The mass spectrometer was operated in the electron ionization (EI) mode at a temperature of 300° C.

Kinetic analysis of reflux reactions

Reaction kinetics were analyzed for the following reactions: hydrochloric acid with vanadyl phthalocyanine, hydrochloric acid with no phthalocyanine, sulfuric acid with vanadyl phthalocyanine and sulfuric acid with no phthalocyanine. Data collected was plotted using traditional chemical kinetic techniques and fitted using the different kinetic models, zero, first or second, to determine the order of the reaction. Samples were studied in 60-minute intervals for a total 6 intervals. Orders of the reactions could be determined by the plotted data fitting into a kinetic model graphically.

Zero-order kinetics models are concluded graphically when plotting the concentration of reactant/product against time results in a straight line defining the zero-order kinetics. Reaction kinetics were plotted using concentrations of resulting products, levulinic methyl ester and heptadionic acid, against time having a slope equal to the positive of the rate constant for the reaction. The integrated rate law is expressed for both products as follows:

$$[LM] - [LM_0] = kt$$

$$[HA] - [HA_0] = kt$$

[LM] is the concentration of levulinic methyl ester at any time, $[LM_0]$ is the concentration of levulinic methyl ester at the start of the reaction, k is the rate constant and t is the time. The same layout would apply for the [HA] and $[HA_0]$ which stands for heptadionic acid at any time and heptadionic acid at the start of the reaction respectively. The units of the rate constant for the zero-order kinetics are $M \cdot s^{-1}$ (concentration·unit of time^{-1}).

For first-order kinetics, the model consists of plotting the natural log of concentration against time resulting in a straight line with the slope equal to the positive of the rate constant for products. The units of the rate constant for the first-order kinetics are s^{-1} (unit of $time^{-1}$). The integrated rate law is expressed for both products as follows:

$$ln\left(\frac{[LM]}{[LM_0]}\right) = kt$$

$$ln\left(\frac{[HA]}{[HA_0]}\right) = kt$$

For second-order kinetics, the model consist of plotting the (1/concentration) against time resulting in a straight line with the slope equal to the negative of the rate constant for products. The units of the rate constant for the second-order kinetics are $M^{-1}{\cdot}s^{-1}$ ($concentration^{-1}{\cdot}$unit of $time^{-1}$). The integrated rate law is express for both products as follows:

$$\frac{1}{[LM]} - \frac{1}{[LM_0]} = -kt$$

$$\frac{1}{[HA]} - \frac{1}{[HA_0]} = -kt$$

Data scatter plots were fitted to the modified kinetic models to determine the order of the reaction[59]. Colum graphs were produced to express the formation of product over time.

CHAPTER IV

RESULTS AND DISCUSSION

FT-IR Results

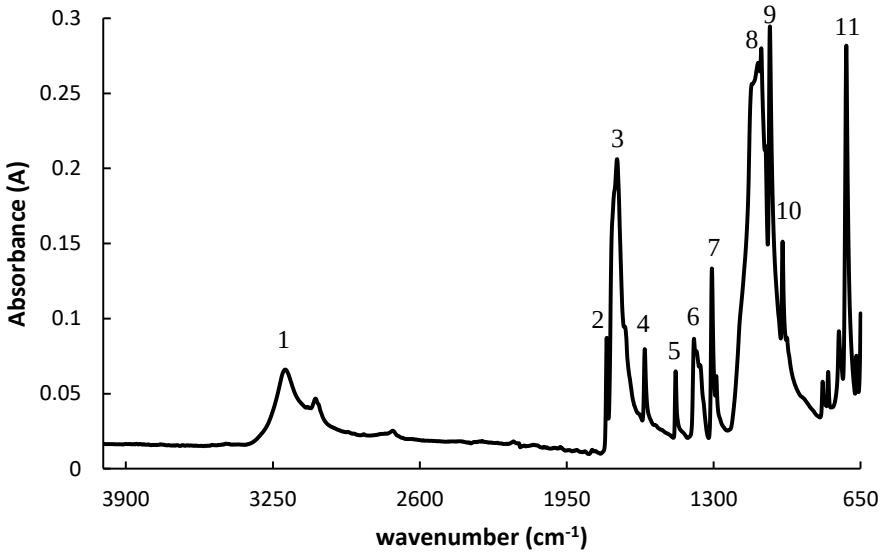

Figure 22. IR spectra of α-H_2Pc

Peak	cm^{-1}	A	Vibration identification
1	3195.43	0.066	N-H bond
2	1773.19	0.0874	-
3	1727.37	0.2063	-
4	1604.8	0.0798	C=C bond
5	1468.18	0.065	Isoindole
6	1386.99	0.0866	-
7	1307.74	0.1337	σ C-H in-plane
8	1089.33	0.2802	σ C-H in-plane

Peak	cm^{-1}	A	Vibration identification
9	1051.31	0.295	σ C-H in-plane+ isoindole
10	995.15	0.1513	σ N-H in plane
11	713.18	0.282	σ C-H out of plane

Table 2. IR peak identification of α-H_2Pc[60]

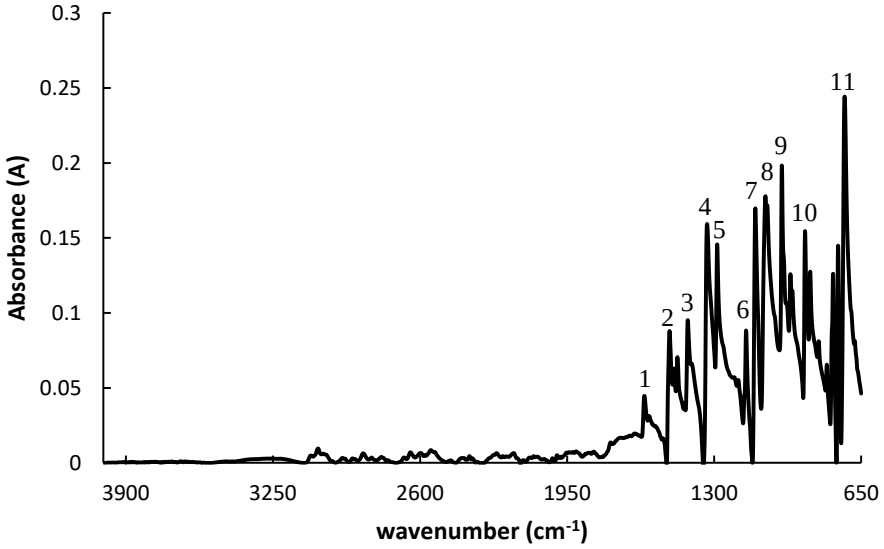

Figure 23. IR spectra of synthesized VOPc

Peak	cm^{-1}	A	Vibration identification
1	1608.65	0.0447	-
2	1497.04	0.088	nitrogen bridging mesoatoms
3	1416.74	0.0953	-
4	1331.32	0.1594	pyrrole fragments and nitrogen mesoatoms
5	1286.55	0.1464	symmetric isoindole fragments
6	1158.76	0.0885	-
7	1117.93	0.1697	C-H in plane
8	1073.34	0.178	C_{arom}-H in plane
9	1000.65	0.1992	-
10	897.99	0.1545	-
11	723.3	0.2444	C-H out of plane

Table 3. IR peak identification of synthesized VOPc[58]

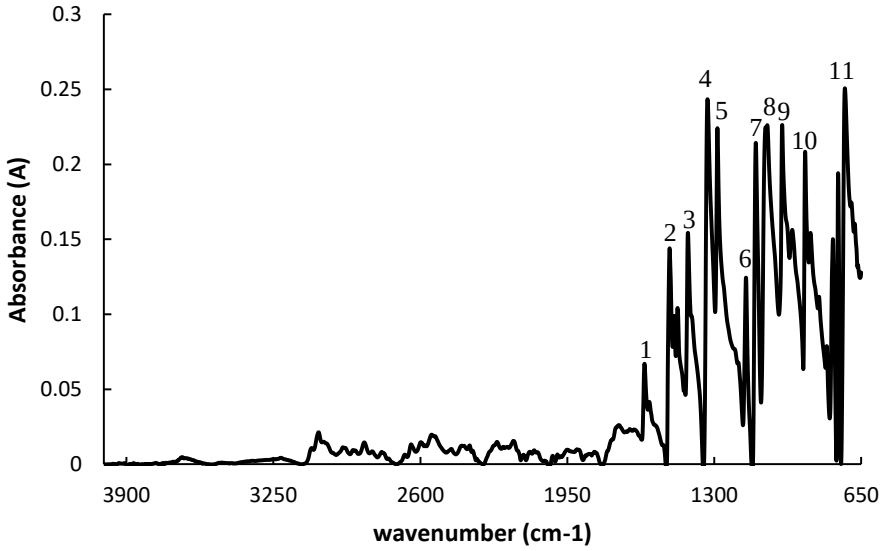

Figure 24. IR spectra of standard reagent-grade VOPc

Peak	cm^{-1}	A	Vibration identificaiton
1	1608.44	0.0672	-
2	1497.23	0.1441	nitrogen bridging mesoatoms
3	1416.5	0.1547	-
4	1329.7	0.2435	pyrrole fragments and nitrogen mesoatoms
5	1285.83	0.2242	symmetric isoindole fragments
6	1159.48	0.125	-
7	1116.15	0.2143	C-H in plane
8	1065.19	0.2262	C_{arom}-H in plane
9	999.54	0.2271	-
10	897.76	0.2088	-
11	721.94	0.2507	C-H out of plane

Table 4. IR peak identification of standard reagent grade VOPc[58]

Infrared (IR) analysis of α metal-free phthalocyanine (α-H_2Pc), synthesized vanadyl phthalocyanine (VOPc) and a standard, reagent grade reference of vanadyl phthalocyanine are shown in Figures 22, 23 and 24 respectively. Each spectra have the peaks labeled with corresponding peaks in the Tables 2,3, and 4 below each spectrum. The identified peaks were

determined from the software and vibrations referenced in literature[58,60]. In the literature, distinct reductions of particular peaks on α-H_2Pc were observed after metalation. Both VOPc samples would indicated metalation of the metal-free phthalocyanine. For the α-H_2Pc IR spectra, peak 1 at 3195.43 cm^{-1} was associated with the N-H vibration of the protons in the center of the molecule. This vibration was not observed in the VOPc molecules indicating the removal of the center protons and indirectly evidence of the addition of the vanadium to the center. In the α-H_2Pc spectra, another peaks indicative of metalation would be peak 9 located at 1051.31 cm^{-1} associated with σ C-H in-plane and isoindole vibrations, which are not present in the VOPc samples further indicating the removal of the center protons and interactions of the vanadium center with surrounding fragments of the phthalocyanine ring.

The VOPc IR spectra's sharp distinct peaks 4 and 5 arise in reference to interactions of nitrogen atoms with the vanadium center within and on the meso position on the phthalocyanine ring. Another indication of the vanadium center having impact on phthalocyanine ring would be fewer broad peaks in comparison with α-H_2Pc and sharper peaks from interactions of the vanadium center with surrounding fragments of the phthalocyanine ring. The disappearance of many in-plane vibrations is a clear indication of the vanadium center being above the phthalocyanine ring plane and disrupting the ring's planer structure. Both spectra for the lab synthesized and standard reagent grade VOPc are in agreement and have similar peak identifications.

XRD Results

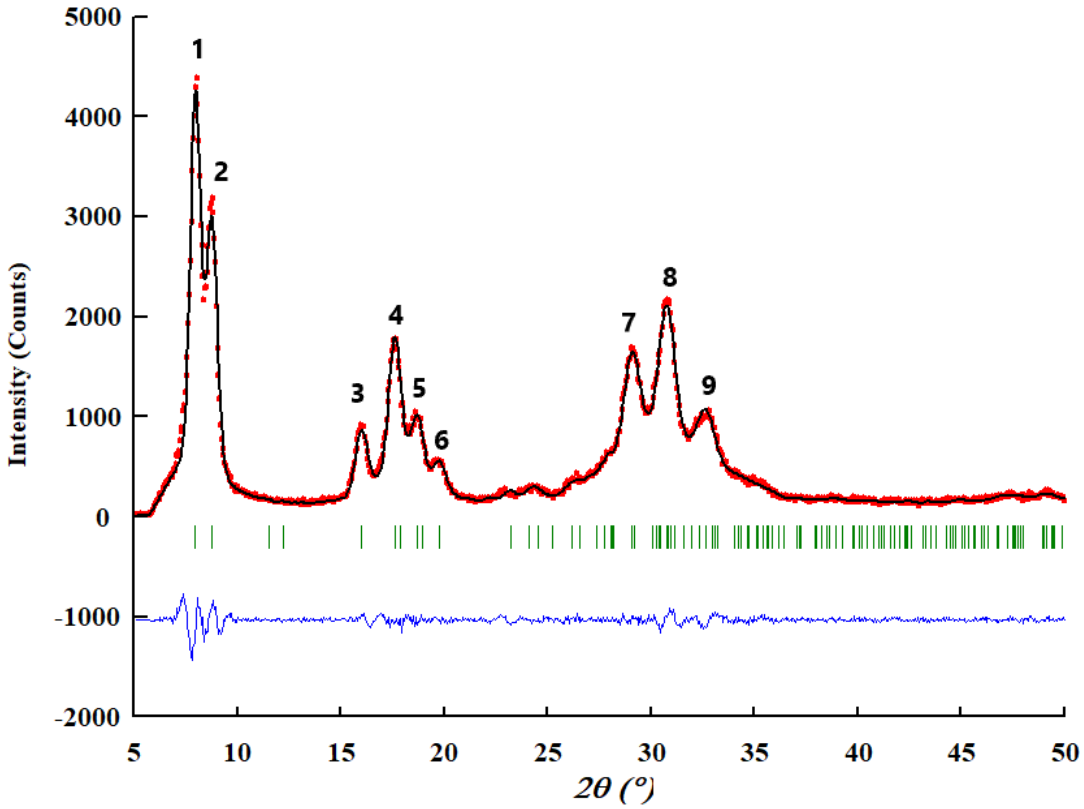

Figure 25. XRD spectra of synthesized α-H_2Pc

Peak	2Θ	Miller indices (hkl)
1	7.9856	(200)
2	8.7913	(002)
3	16.008	(400)
4	17.6327	(004)
5	18.7085	(402)
6	19.7783	(204)

Peak	2Θ	Miller indices (hkl)
7	29.2273	(112)
8	30.9385	(113)
9	32.3375	(-313)

Table 5. XRD peak identification for synthesized α-H_2Pc

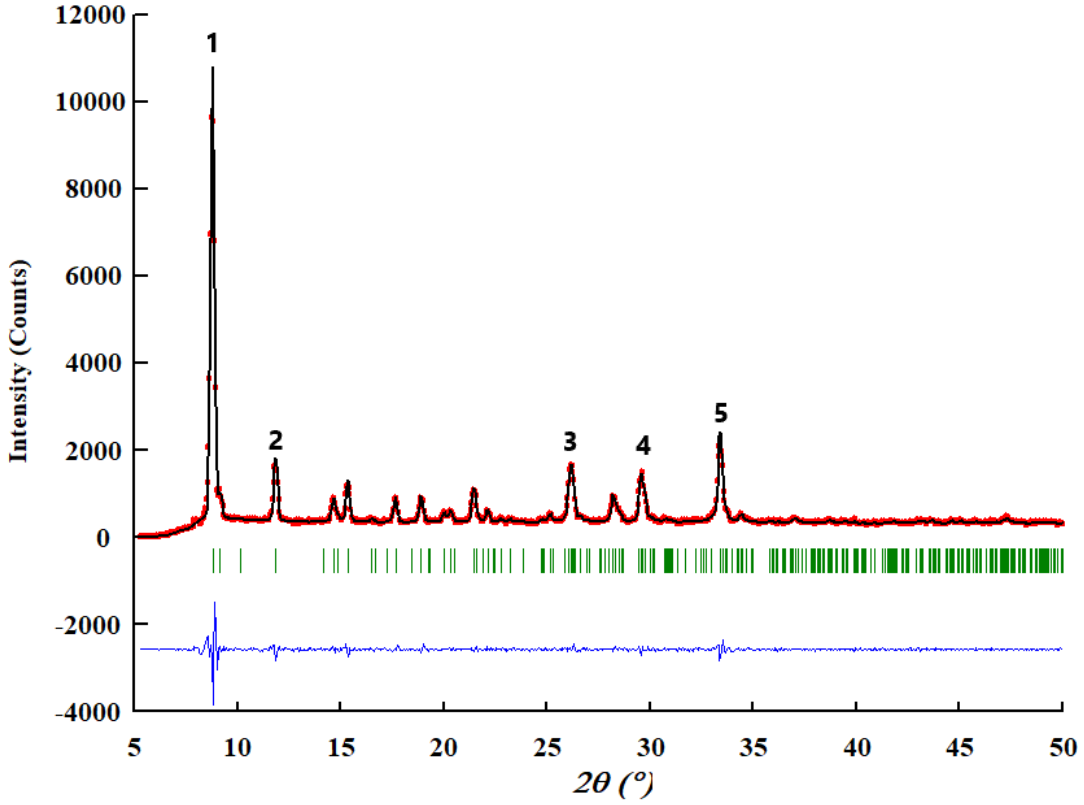

Figure 26. XRD spectra of synthesized VOPc

Peak	2Θ	Miller indices (hkl)
1	8.8065	(010)
2	11.8674	(001)
3	26.1694	(012)
4	29.6488	(-2-22)
5	33.3852	(222)

Table 6. XRD peak identification for synthesized VOPc

Compound	Space Group	a (Å)	b (Å)	c (Å)	α (°)	β (°)	γ (°)	$^{*}\chi^2$ (GOF)
α-H_2Pc_{samp}	C_2/n	25.755	3.773	23.398	90	93.111	90	2.068
α-H_2Pc_{lit}	C_2/n	26.121	3.797	23.875	90	94.16	90	-
$VOPc_{samp}$	P-1	12.058	12.598	8.719	96.203	94.941	68.204	1.671
$VOPc_{lit}$	P-1	12.027	12.571	8.690	96.04	94.80	68.20	-

Table 7. Comparison of Fullprof fitting parameters of synthesized samples to literature[55,56,57]

$^{*}\chi^2$ GOF (goodness of fit) with a value less than 5 is an accepted fitting

The LeBail fitted X-ray powder diffraction (XRD) analysis of α-H_2Pc and synthesized VOPc are shown in Figure 25 and 26, respectively. Each diffraction pattern uses the following legend: red dots – sample pattern, black line – fitted pattern, blue line – sample and fitted pattern difference, and green lines – Braggs planes. At the bottom of the spectra, Tables 5 and 6 indicate the diffraction angle in 2Θ and the identified Miller indices for each peak using the Fullprof software. Table 7 summarizes and compares sample parameters to those found in literature[55,56,57].

For the synthesized α-H_2Pc, the compound exhibits a C_2/n space group, which is a monoclinic crystal structure and C_{2h} point group linking to planar symmetry features of cyclic system with σ_h mirror plane. As shown on Table 7, α-H_2Pc_{samp} lattice parameters closely resemble those found in literature labeled α-H_2Pc_{lit} and has a χ^2 of 2.068 which less than 5 making this an accepted fitting. From literature, α-H_2Pc exhibits peaks in 2Θ at angles of 6.79°, 14.9° and 26.4° with Miller indices of (200), (004) and (113) respectively[55,56].

For synthesized VOPc, the compound exhibits a P-1 space group indicating a triclinic crystal structure and the absence of any symmetry features exhibiting only C_1 symmetry due to

the cyclic geometry. The lack of symmetry is due to the vanadyl phthalocyanine compound not having planar geometry and the vanadium center located above plane disrupting all other attached molecules[57]. The lattice parameters shown in Table 7 are similar for $VOPc_{samp}$ and $VOPc_{lit}$ with sample χ^2 being 1.671, which indicates an excellent agreement between the fitting and literature. From literature, the distinct peak associated with VOPc would be at 2Θ angle = 7.4° with Miller indices (010) corresponding with triclinic crystal structure. Other possible weak peaks could be seen at angles 12.5°, 15° and 22.4°[58].

GC-MS Results

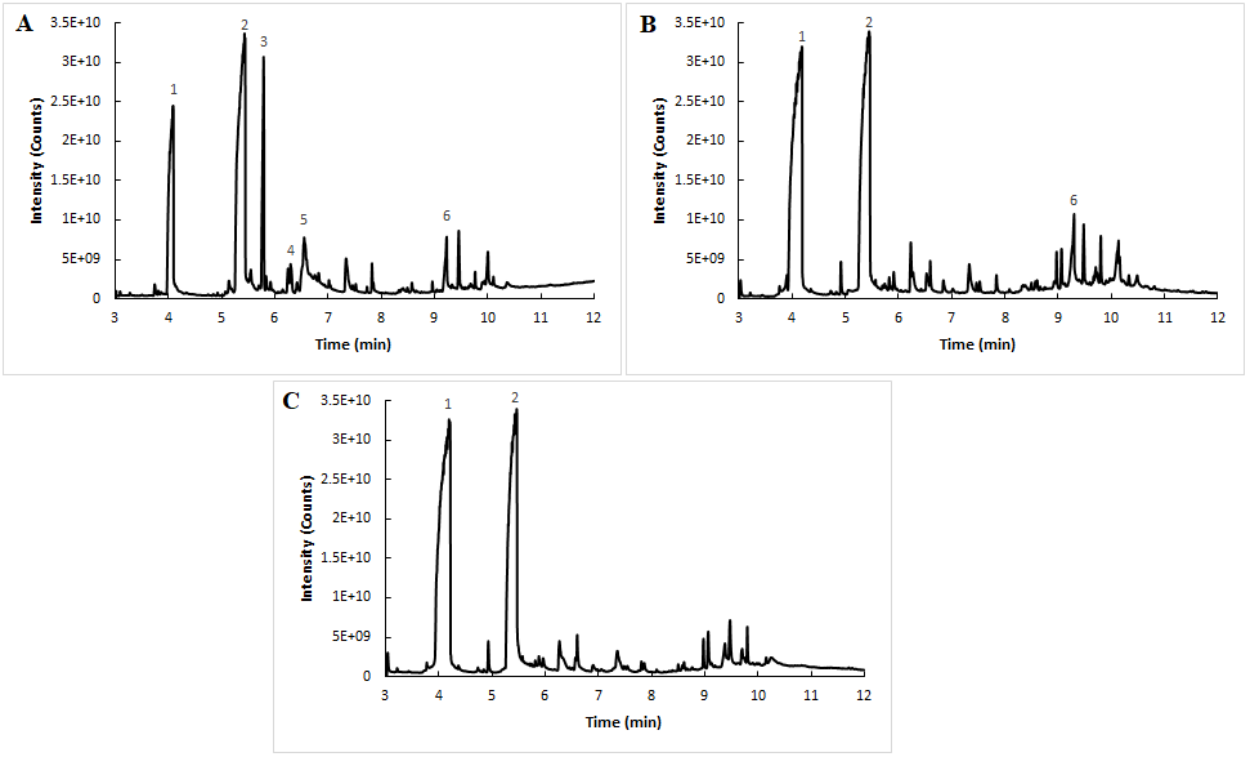

Figure 27. GC-MS spectra of HCl reactions

Peak	RT	Identification	CAS No.
1	4.09	methyl levulinate	624-45-3
2	5.43	2,4-heptadienoic acid	56424-97-6
3	5.79	-	-
4	6.29	hexoxyacetaldehyde dimethyl acetal	17597-95-4
5	6.55	5-hydroxymethyl-2-furancarbaldehyde	67-47-0
6	9.30	palmitic acid	57-10-3

Table 8. GC-MS peak identification for HCl reactions

Figure 27 shows gas chromatography with mass spectroscopy (GC-MS) spectra of catalytic reactions of fructose with VOPc using hydrochloric acid (HCl) sampled at 8 (A), 16 (B)

and 24 (C) hours. Spectra display dominant peaks 1 and 2 over time corresponding to major products methyl levulinate and 2,4-heptadienoic acid as seen on Table 8 at retention times (RT) of 4.09 min and 5.43 min respectively. Other peak identifications were confirmed using the GC-MS database and could be seen in Table 8.

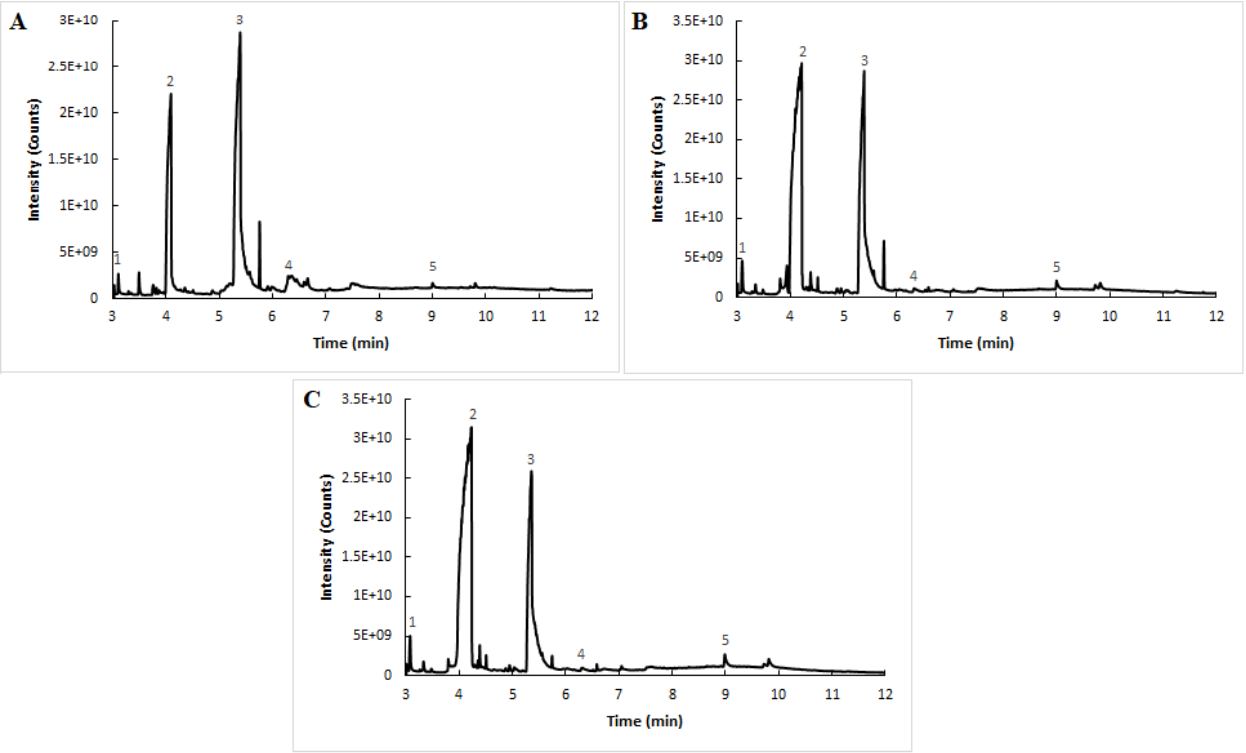

Figure 28. GC-MS spectra of H_2SO_4 reactions

Peak	RT	Identification	CAS No.
1	3.10	Methyl dimethoxyacetate	89-91-8
2	4.08	Methyl levulinate	624-45-3
3	5.39	2,4-heptadienoic acid	56424-97-6
4	6.36	-	-
5	9.00	methyl palmitate	112-39-0

Table 9. GC-MS peak identification for H_2SO_4 reactions

Figure 28 shows GC-MS spectra of catalytic reactions of fructose with VOPc using sulfuric acid (H_2SO_4) sampled at 8, 16 and 24 hours. Spectra display dominant peaks 2 and 3 over time corresponding to major products methyl levulinate and 2,4-heptadienoic acid as seen on Table 9 at RT of 4.08 min and 5.39 min respectively. Other peak identifications were confirmed using the GC-MS database and could be seen in Table 9.

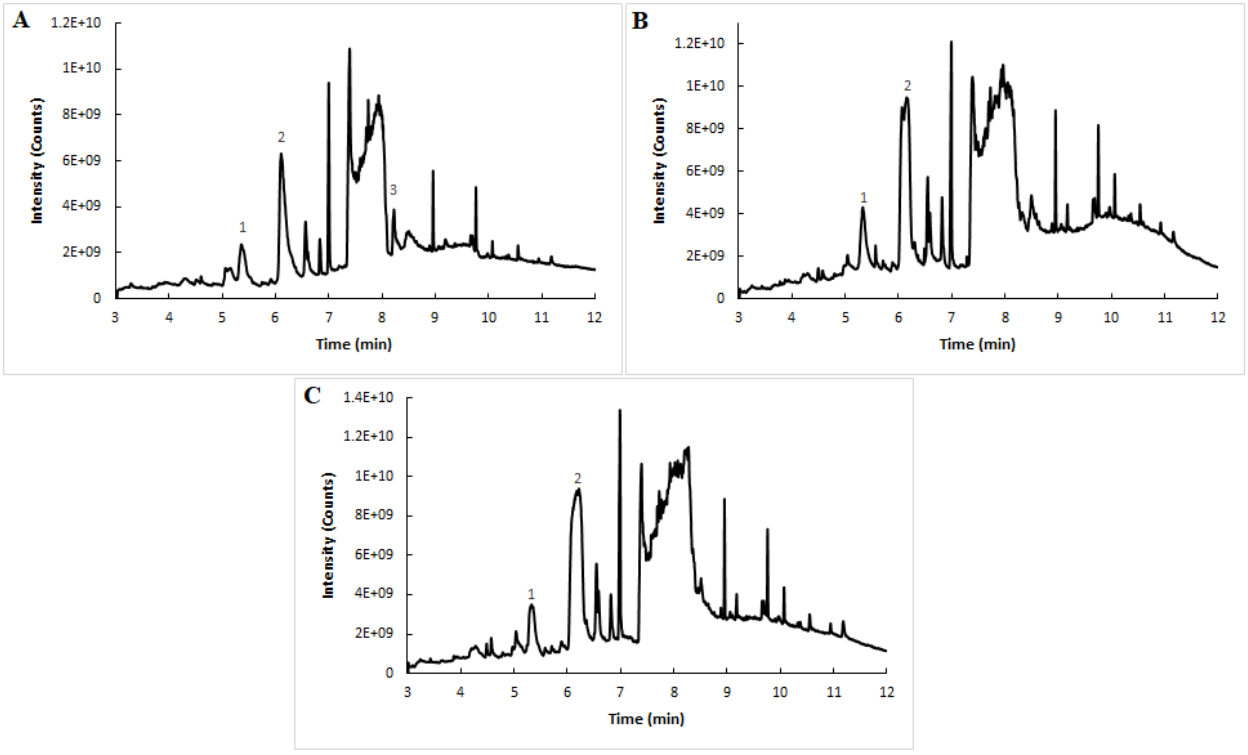

Figure 29. GC-MS spectra of HNO_3 reactions

Peak	RT	Identification	CAS No.
1	5.33	2,4-dihydroxy-2,5-dimethyl-3(2H)-furanone	10230-62-3
2	6.22	5-hydroxymethyl-2-furancarbaldehyde	67-47-0
3	8.28	2-cyanobenzoic acid	3839-22-3

Table 10. GC-MS peak identification for HNO_3 reactions

Figure 29 shows GC-MS spectra of catalytic reactions of fructose with VOPc using nitric acid (HNO_3) sampled at 8, 16 and 24 hours. Spectra display mixture of products over time with many being unable to identify with possibilities obtained for the GC-MS database are shown in Table 10.

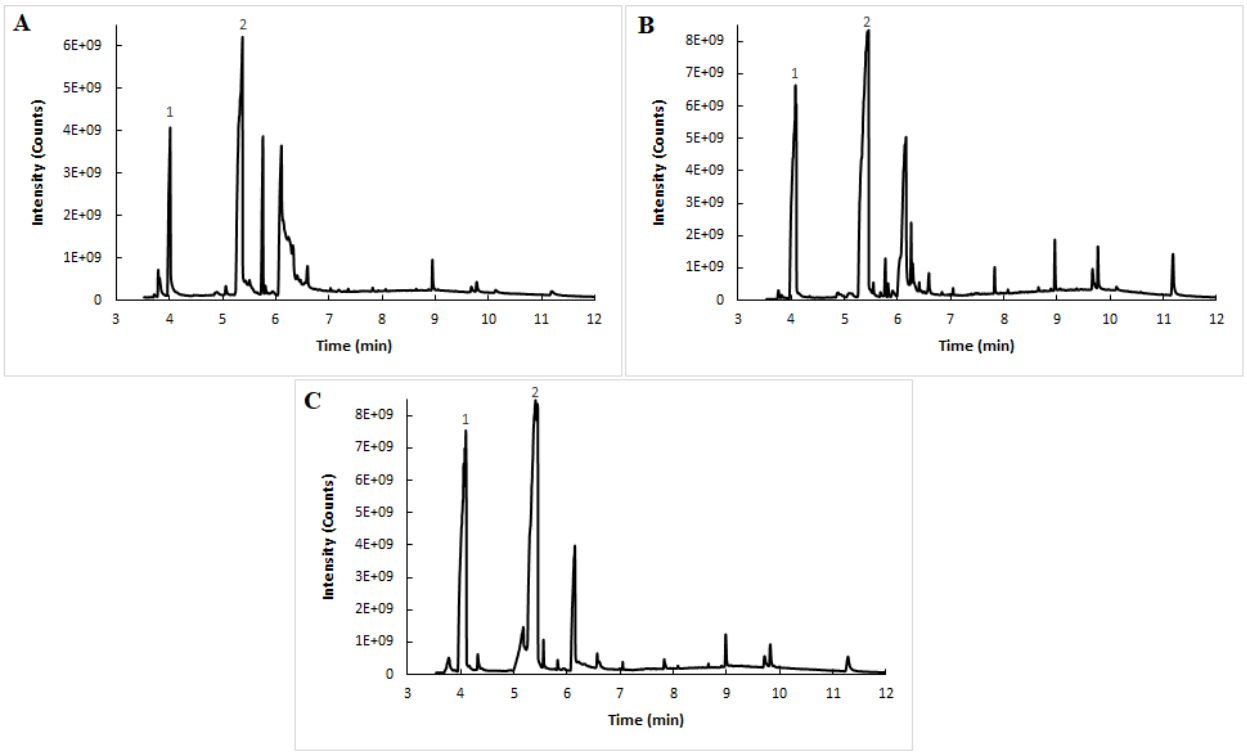

Figure 30. GC-MS spectra of HBr reactions

Peak	RT	Identification	CAS No.
1	4.03	Methyl levulinate	624-45-3
2	5.36	2,4-heptadienoic acid	56424-97-6

Table 11. GC-MS peak identification for HBr reactions

Figure 30 shows GC-MS spectra of catalytic reactions of fructose with VOPc using hydrobromic acid (HBr) sampled at 8, 16 and 24 hours. Spectra display dominant peaks 1 and 2 over time corresponding to major products methyl levulinate and 2,4-heptadienoic acid as seen on Table 11 at RT of 4.03 min and 5.36 min respectively.

From the data collected using different conditions for the catalytic reactions, HCl and H_2SO_4 demonstrated favorable conditions producing major products in higher counts within the 24 hours of sampling. The optimization of reactions, HCl and H_2SO_4 reactions, were replicated with the addition of control reactions run without VOPc.

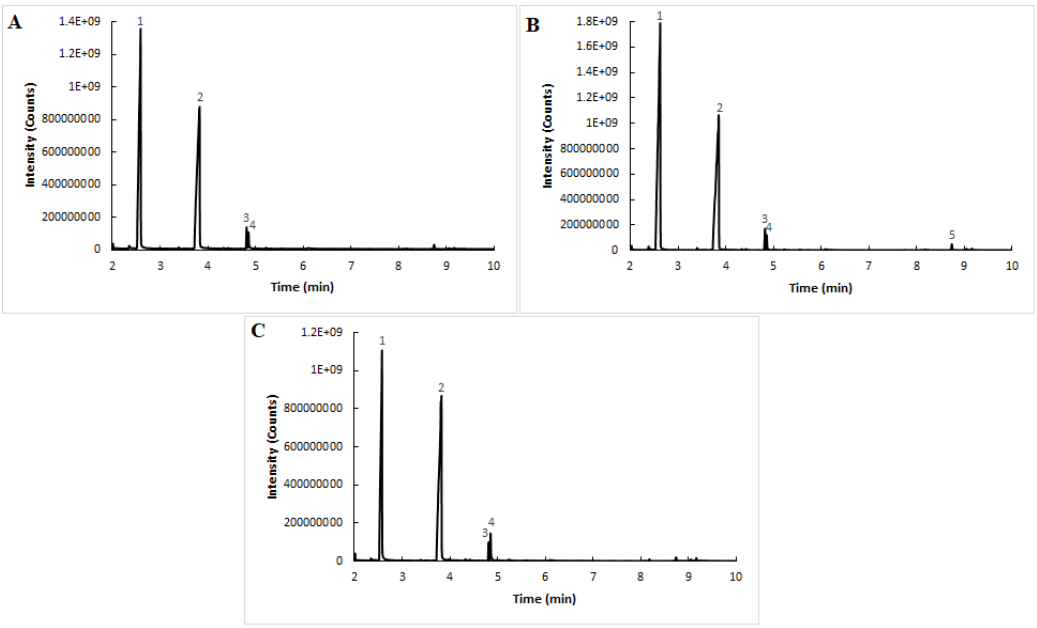

Figure 31. GC-MS spectra of replicated HCl reactions with VOPc

A	RT	Area	Area %
Peak 1	2.594	5.74E+07	48.94
Peak 2	3.829	5.65E+07	48.15
Peak 3	4.81	1.86E+06	1.58
Peak 4	4.85	1.56E+06	1.33

B	RT	Area	Area %
Peak 1	2.619	9.54E+07	54.66
Peak 2	3.844	7.39E+07	42.34
Peak 3	4.815	2.70E+06	1.55
Peak 4	4.855	1.65E+06	0.95
Peak 5	8.736	9.01E+05	0.52

C	RT	Area	Area %
Peak 1	2.579	3.73E+07	40.24
Peak 2	3.824	5.19E+07	55.91
Peak 3	4.81	1.36E+06	1.47
Peak 4	4.85	2.21E+06	2.39

Figure 32. Data tables for replicated HCl reactions with VOPc

Figure 31 shows GC-MS spectra for replicated HCl reactions with samples at 8 (A), 16 (B) and 24 (C) hours. Figure 32 displays a compilation of tables for each sample with its contributing area and area % for the peak. In these spectra, peak 1 would be methyl levulinate and peak 2 would be 2,4-heptadienoic acid. Other peaks were unidentifiable and labeled for distribution of area for the spectra.

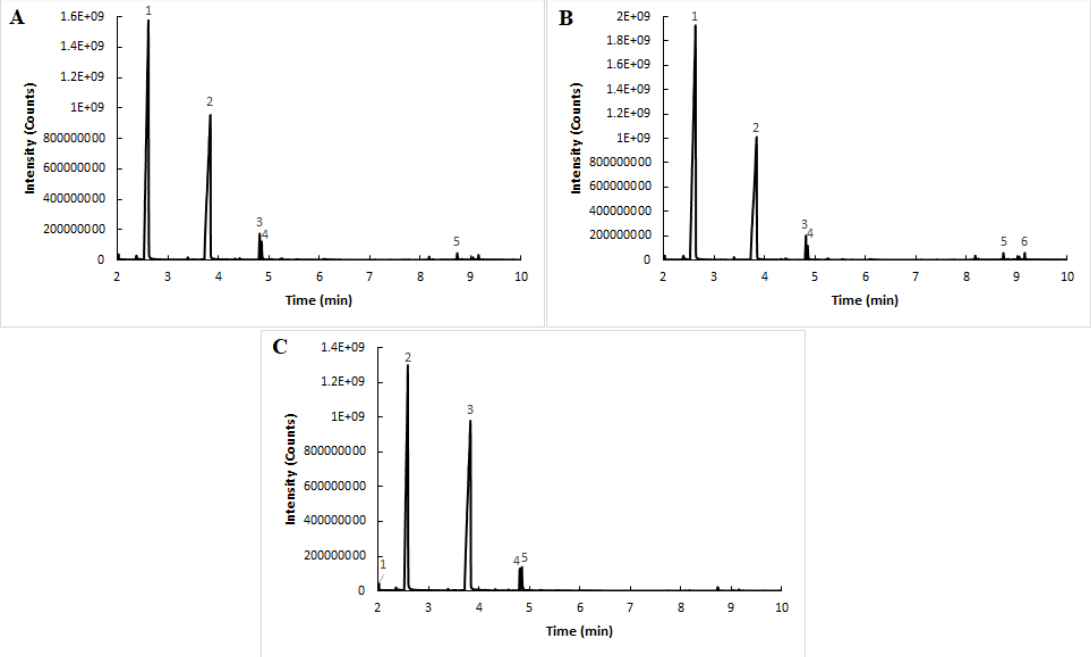

Figure 33. GC-MS spectra for control HCl reactions without VOPc

A	RT	Area	Area %
Peak 1	2.609	7.91E+07	53.22
Peak 2	3.834	6.47E+07	43.48
Peak 3	4.815	2.31E+06	1.56
Peak 4	4.85	1.78E+06	1.19
Peak 5	8.731	8.15E+05	0.55

B	RT	Area	Area %
Peak 1	2.624	1.15E+08	61.26
Peak 2	3.839	6.66E+07	35.42
Peak 3	4.815	2.87E+06	1.52
Peak 4	4.85	1.49E+06	0.79
Peak 5	8.731	1.05E+06	0.56
Peak 6	9.156	8.29E+05	0.44

C	RT	Area	Area %
Peak 1	2.018	2.26E+05	0.19
Peak 2	2.589	5.23E+07	43.04
Peak 3	3.829	6.52E+07	53.62
Peak 4	4.81	1.79E+06	1.47
Peak 5	4.85	2.05E+06	1.68

Figure 34. Data tables for control HCl reactions without VOPc

Figure 33 shows GC-MS spectra for control HCl reactions with no VOPc with samples at 8, 16 and 24 hours. Figure 34 displays a compilation of tables for each sample with its contributing area and area % for the peak. In these spectra, peak 1 would be methyl levulinate

and peak 2 would be 2,4-heptadienoic acid until spectra C where identification would shift over 1 peak with peak 2 being methyl levulinate and peak 3 being 2,4-heptadienoic acid. Other peaks were unidentifiable and labeled for distribution of area for the spectra.

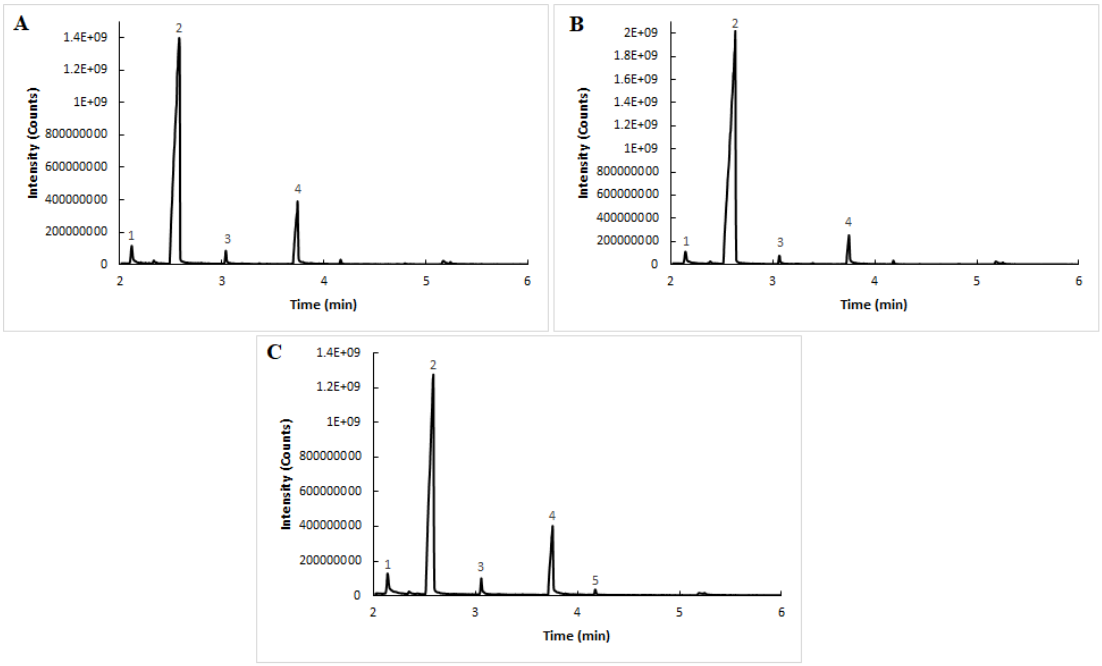

Figure 35. GC-MS spectra of replicated H_2SO_4 reactions with VOPc

A	RT	Area	Area %
Peak 1	2.118	2.41E+06	2.53
Peak 2	2.584	7.99E+07	83.81
Peak 3	3.039	1.36E+06	1.43
Peak 4	3.744	1.17E+07	12.23

B	RT	Area	Area %
Peak 1	2.138	2.95E+06	2.20
Peak 2	2.629	1.24E+08	92.57
Peak 3	3.059	1.35E+06	1.01
Peak 4	3.744	5.64E+06	4.22

C	RT	Area	Area %
Peak 1	2.133	3.46E+06	4.59
Peak 2	2.584	5.72E+07	76.08
Peak 3	3.054	1.62E+06	2.15
Peak 4	3.754	1.24E+07	16.51
Peak 5	4.169	5.06E+05	0.67

Figure 36. Data tables for replicated H_2SO_4 reactions with VOPc

Figure 35 shows GC-MS spectra of replicated H_2SO_4 reactions with VOPc with samples at 8, 16 and 24 hours. Figure 36 displays a compilation of tables for each sample with its contributing area and area % for the peak. In these spectra, peak 2 would be methyl levulinate and peak 4 would be 2,4-heptadienoic acid. Other peaks were unidentifiable and labeled for distribution of area for the spectra.

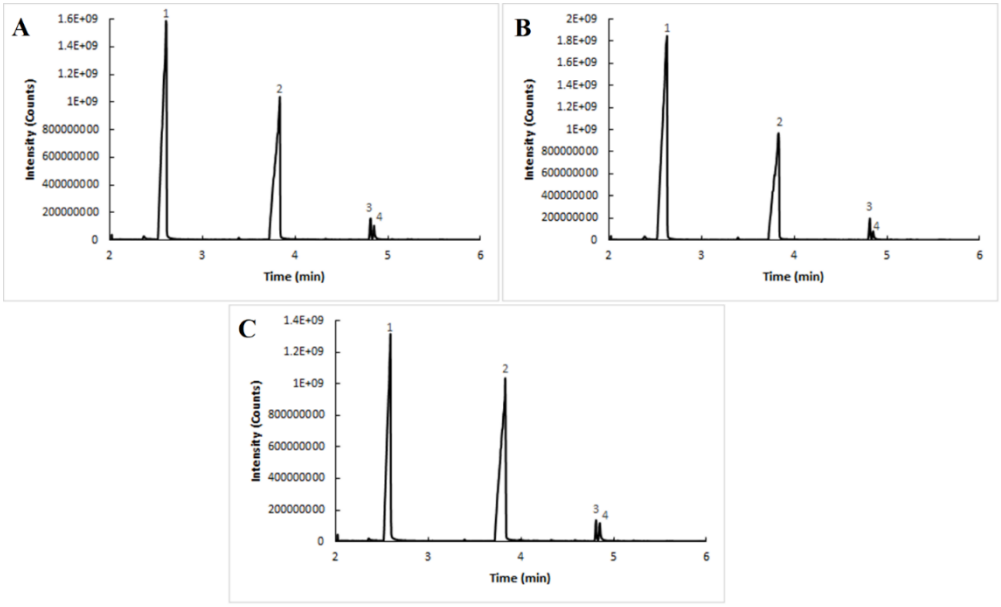

Figure 37. GC-MS spectra of control H_2SO_4 reactions without VOPc

A	RT	Area	Area %
Peak 1	2.604	8.03E+07	48.79
Peak 2	3.834	8.03E+07	48.79
Peak 3	4.815	2.45E+06	1.49
Peak 4	4.85	1.52E+06	0.92

B	RT	Area	Area %
Peak 1	2.624	1.08E+08	62.42
Peak 2	3.829	6.10E+07	35.32
Peak 3	4.815	2.75E+06	1.59
Peak 4	4.85	1.16E+06	0.67

C	RT	Area	Area %
Peak 1	2.589	5.29E+07	46.02
Peak 2	3.829	5.83E+07	50.72
Peak 3	4.81	1.88E+06	1.63
Peak4	4.85	1.87E+06	1.62

Figure 38. Data tables for control H_2SO_4 reactions without VOPc

Figure 37 shows GC-MS spectra of control H_2SO_4 reactions without VOPc with samples at 8, 16 and 24 hours. Figure 38 displays a compilation of tables for each sample with its contributing area and area % for the peak. In these spectra, peak 1 would be methyl levulinate and peak 2 would be 2,4-heptadienoic acid. Other peaks were unidentifiable and labeled for distribution of area for the spectra.

The replicated and control reactions for both acids confirmed tendencies for production of desired products. For HCl reactions, both replica and control have methyl levulinate and 2,4-heptadienoic acid production nearly the same with both trials having a reduction in methyl levulinate output. The reduction occurs passing the 16-hour mark into the 24-hour sample in reference to area, but counts are still significantly high. For H_2SO_4 reactions, both replica and control have methyl levulinate and 2,4-heptadienoic acid production showing preferred production of the methyl levulinate over 2,4-heptadienoic acid suggesting favorability. Both replica and control favored the production of methyl levulinate more than the 2,4-heptadienoic acid. Kinetic reactions were performed to determine the production of desired products at the beginning of the reactions rather than at 24-hour of reaction

Kinetic Results

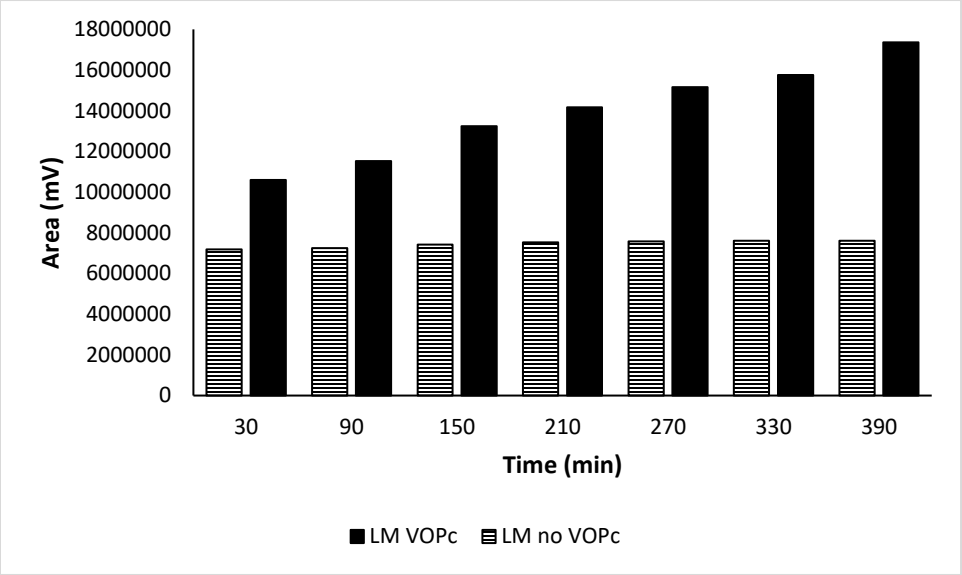

Figure 39. Kinetic results for H_2SO_4 reactions

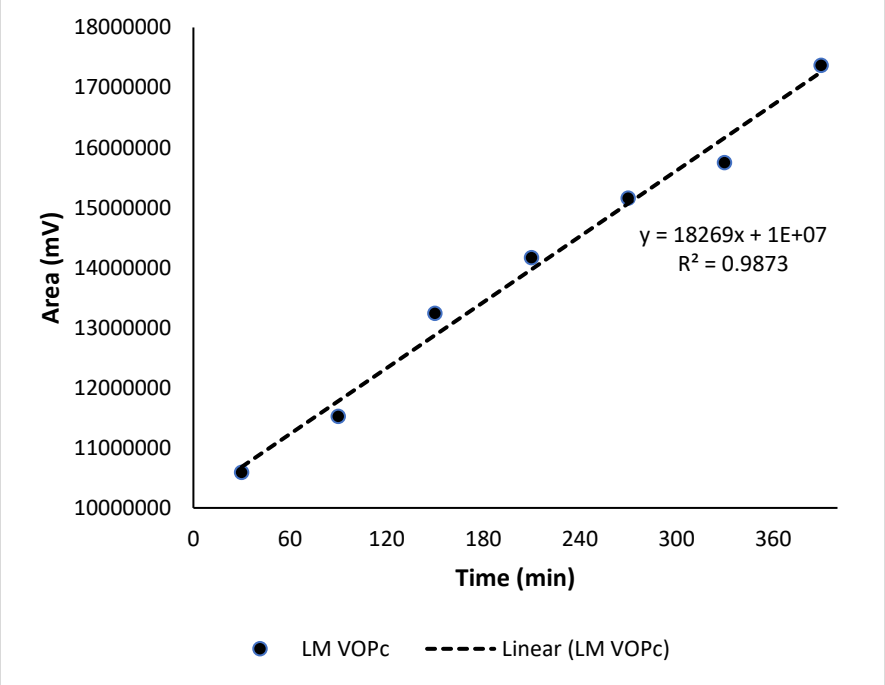

Figure 40. Kinetic plot for H_2SO_4 reactions with VOPc

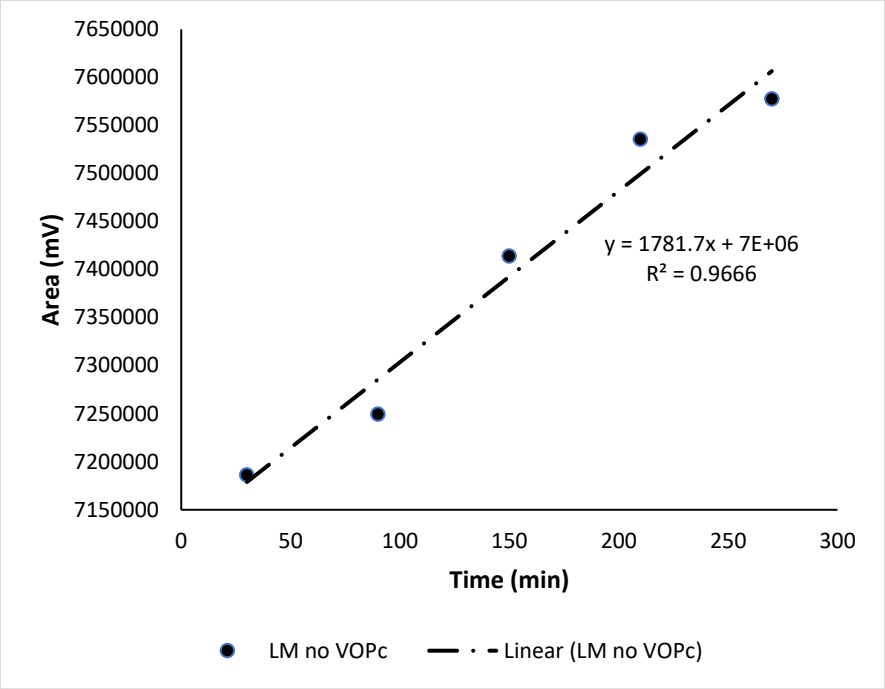

Figure 41. Kinetic plot for H_2SO_4 reactions without VOPc

Figure 39 shows the kinetic results to produce levulinic methyl ester (LM) over a time span of 6.5 hours with 30-minute sampling intervals in the presence of VOPc and in the absence of VOPc. The absence of 2,4-heptadienoic acid (HA) agrees with the GC-MS data being selective in H_2SO_4 reactions. HA production was not factored into kinetic results or plot for H_2SO_4 reaction. Both results and plots show H_2SO_4 reactions with VOPc being favorable to produce LM. Figures 40 and 41 display kinetic plot data for H_2SO_4 reactions with or without VOPC respectively. Each plot was graphed using area against time and agreeing with the zero-order kinetic model with high R^2 and having a positive slope in accordance with the kinetic equation below:

$$[LM] - [LM_0] = kt$$

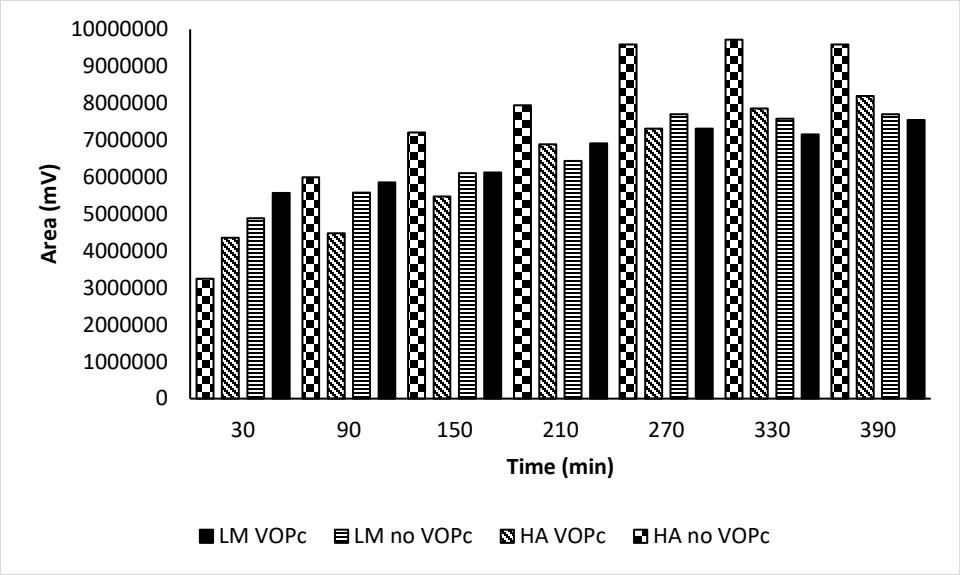

Figure 42. Kinetic results for HCl reactions

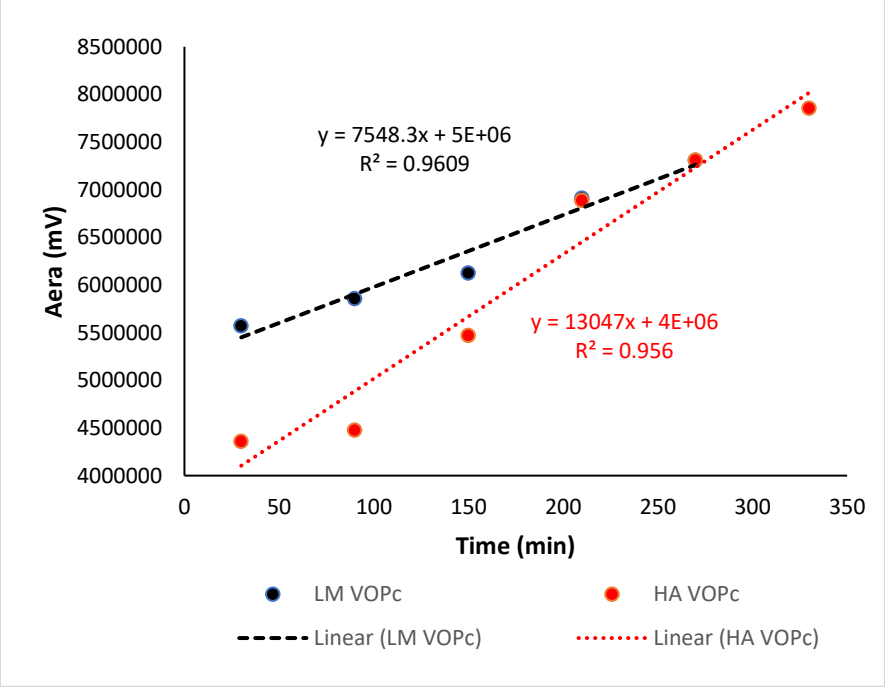

Figure 43. Kinetic plot for HCl reactions with VOPc

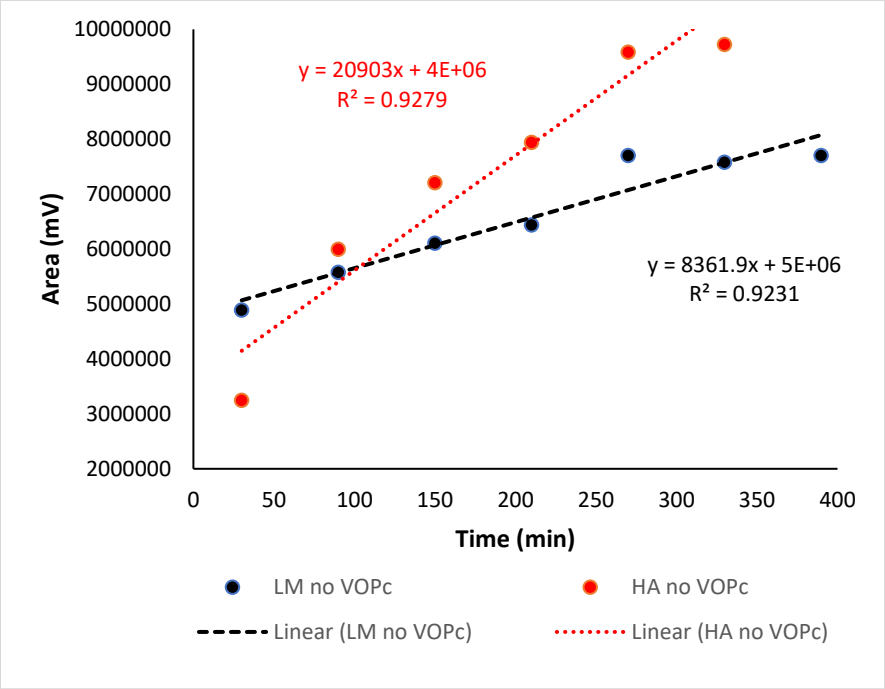

Figure 44. Kinetic plot for HCl reactions without VOPc

Figure 42 shows the kinetic results to produce LM and HA over a time span of 6.5 hours with 30-minute intervals with and without VOPc. The results show HCl reactions with VOPc being favorable in production of LM early in the reaction and have a constant output throughout. The production of HA increases significantly as time progresses especially in the absence of VOPc and does not show consistent readouts. Figures 43 and 44 display kinetic plot data for HCl reactions with or without VOPC respectively. Each plot was graphed using area against time and agreeing with the zero-order kinetic model with high R^2 and having a positive slope in accordance with the kinetic equation below:

$$[LM] - [LM_0] = kt$$

$$[HA] - [HA_0] = kt$$

The kinetic data shows the selectivity to produce LM in H_2SO_4 reactions. Where as HCl reactions, the production of LM was higher early in the reactions with VOPC and tend to shift to more production of HA with in the 6.5-hour time span. As for the reactions without VOPc, HA production was higher for most of the time surpassing the making of LM.

CHAPTER V

CONCLUSION

Synthesized α-H_2Pc and VOPc were characterized by IR spectroscopy confirming the metalation of the metal-free phthalocyanine with vanadium with appearance and disappearance of certain peaks that are features of each molecule. IR spectra for synthesized VOPc was referenced to a standard sample of VOPc to be in agreement with all peaks being similar. XRD analysis further validated the alpha form of metal-free phthalocyanine and vanadyl phthalocyanine when comparing lattice parameters from literature matched and χ^2 values were below 5, 2.068 and 1.671 respectively, confirming good agreement between the data and the literature.

After classification of synthesized VOPc, reflux reactions using the catalyst were performed using fructose, several acids, and methanol as a solvent. HCl and H_2SO_4 reactions had promising results producing the desired products, levulinic methyl ester and 2,4-heptadienoic acid, as determined using GC-MS data from samples monitored within 24 hours. HBr showed the formation of desired products but did not have the concentrations as those observed with the HCl and H_2SO_4 catalyzed reactions. HNO_3 had no oxidation of desired products. Results were replicated for both acids and referenced to a control without VOPc to view if catalyst was optimal for the producing desired product within 24 hours. The combination of H_2SO_4 and VOPc proved to be selective on produce levulinic methyl ester over 2,4-heptadienoic acid by

suppressing the appearance of the peak shown in GC-MS spectra. The combination of HCl and VOPc showed similar spectra for both products for reactions with and without VOPc.

Kinetic reactions results showed the same trend with the combination of H_2SO_4 and VOPc having lower production of HA and higher output of LM than without VOPc over a 6.5-hour period. For the combination of HCl and VOPc, early results showed higher production of LM with HA production gradually reaching similar amounts while HCl reactions without VOPc tend to produce greater amounts of HA thru the entire time period. All kinetic plots showed zero-order kinetics.

Further investigation is needed to expand optimal reaction conditions using vanadyl phthalocyanine to generate levulinic methyl ester and 2,4-heptadienoic acid from oxidation of sugar molecules using the parameters and data found in this study. Replication, instrumentation, time sensitivity and reflux conditions can be reevaluated for future findings on the topic of using phthalocyanines for the oxidation of sugars as this study has shown it to be possible.

REFERENCES

1. Leznoff, C. C.; P., L. A. B. *Phthalocyanines: properties and applications*; VCH: New York, NY, 1996; Vol. 4

2. Braun, A.; Tcherniac, J. Über Die Produkte Der Einwirkung Von Acetanhydrid Auf Phthalamid. *Berichte der deutschen chemischen Gesellschaft* 1907, *40* (2), 2709–2714

3. de Diesbach, H.; Sehmidt, V.; Decker, E. Une Préparation Simple De L'acide Pyromellithique. *Helvetica Chimica Acta* 1923, *6* (1), 548–549

4. Linstead, R. P. *British Association for the Advancement of Science* 1933, 465–466

5. Linstead, R. P. 212. Phthalocyanines. Part I. A New Type of Synthetic Colouring Matters. *Journal of the Chemical Society (Resumed)* 1934, 1016–1017

6. Linstead, R. P.; Lowe, A. R. 214. Phthalocyanines. Part III. Preliminary Experiments on the Preparation of Phthalocyanines from Phthalonitrile. *Journal of the Chemical Society (Resumed)* 1934, 1022–1027

7. Linstead, R. P.; Lowe, A. R. 216. Phthalocyanines. Part V. The Molecular Weight of Magnesium Phthalocyanine. *Journal of the Chemical Society (Resumed)* 1934, 1031–1033

8. Klüver, H.; Barrera, E. On the Use of Azaporphin Derivatives (Phthalocyanines) in Staining Nervous Tissue. *The Journal of Psychology* 1954, *37* (2), 199–223

9. Dahlen, M. A. The Phthalocyanines: A New Class of Synthetic Pigments and Dyes. *Industrial & Engineering Chemistry* 1939, *31* (7), 839–847

10. Smith, K. M. Porphyrins, Corrins and Phthalocyanines. *Comprehensive Heterocyclic Chemistry* 1984, 377–442

11. Eguchi, K.; Nakagawa, T.; Takagi, Y.; Yokoyama, T. Direct Synthesis of Vanadium Phthalocyanine and Its Electronic and Magnetic States in Monolayers and Multilayers on Ag(111). *The Journal of Physical Chemistry C* 2015, *119* (18), 9805–9815

12. Eley, D. D. Phthalocyanines as Semiconductors. *Nature* 1948, *162* (4125), 819–819

13. Hains, A. W.; Liang, Z.; Woodhouse, M. A.; Gregg, B. A. Molecular Semiconductors in Organic Photovoltaic Cells. *Chemical Reviews* 2010, *110* (11), 6689–6735

14. Moser, F. H.; Thomas, A. L. *Phthalocyanine compounds*; Reinhold: New York, 1963

15. Sorokin, A.; Meunier, B. Oxidative Degradation of Polychlorinated Phenols Catalyzed by Metallosulfophthalocyanines. *Chemistry - A European Journal* 1996, *2* (10), 1308–1317

16. Ortiz de Montellano, P. R. *Cytochrome P450: structure, mechanism, and biochemistry*, 3rd ed.; Kluwer Academic/Plenum Publishers: New York, NY, 2005

17. Mulder, G. J. Untersuchungen Über Die Humussubstanzen. *Journal für Praktische Chemie* 1840, *21* (1), 321–370

18. Girisuta, B.; Janssen, L. P. B. M.; Heeres, H. J. Green Chemicals. *Chemical Engineering Research and Design* 2006, *84* (5), 339–349

19. Rackemann, D. W.; Doherty, W. O. S. The Conversion of Lignocellulosics to Levulinic Acid. *Biofuels, Bioproducts and Biorefining* 2011, *5* (2), 198–214

20. Peng, L.; Lin, L.; Li, H.; Yang, Q. Conversion of Carbohydrates Biomass into Levulinate Esters Using Heterogeneous Catalysts. *Applied Energy* 2011, *88* (12), 4590–4596

21. Olson, E. S.; Kjelden, M. R.; Schlag, A. J.; Sharma, R. K. Levulinate Esters from Biomass Wastes. *ACS Symposium Series* 2001, 51–63

22. Leonard, R. H. Levulinic Acid as a Basic Chemical Raw Material. *Industrial & Engineering Chemistry* 1956, *48* (8), 1330–1341

23. Chang, C.; Xu, G.; Jiang, X. Production of Ethyl Levulinate by Direct Conversion of Wheat Straw in Ethanol Media. *Bioresource Technology* 2012, *121*, 93–99

24. Le Van Mao, R.; Zhao, Q.; Dima, G.; Petraccone, D. New Process for the Acid-Catalyzed Conversion of Cellulosic Biomass (AC_3B) into Alkyl Levulinates and Other Esters Using a Unique One-Pot System of Reaction and Product Extraction. *Catalysis Letters* 2010, *141* (2), 271–276

25. Sowden, J. C. The Action of Hydrobromic Acid on 1-C^{14}-D-Glucose. *Journal of the American Chemical Society* 1949, *71* (10), 3568–3568

26. Grote, A. F.; Tollens, B. Untersuchungen Über Kohlenhydrate. I. Ueber Die Bei Einwirkung Von Schwefelsäure Auf Zucker Entstehende Säure (Levulinsäure). *Justus Liebig's Annalen der Chemie* 1875, *175* (1-2), 181–204

27. Grote, A.; Tollens, B. II. Ueber Die Bildung Von Lävulinsäure Aus Verschiedenen Kohlehydraten. Entstehung Der Lävulinsäure Aus Dextrose. *Justus Liebig's Annalen der Chemie* 1881, *206* (1-2), 226–232

28. Thomas, R. W.; Schuette, H. A. STUDIES ON LEVULINIC ACID. I. ITS PREPARATION FROM CARBOHYDRATES BY DIGESTION WITH HYDROCHLORIC ACID UNDER PRESSURE. *Journal of the American Chemical Society* 1931, *53* (6), 2324–2328

29. Antal, M. J.; Mok, W. S. L.; Richards, G. N. Mechanism of Formation of 5-(Hydroxymethyl)-2-Furaldehyde from d-Fructose and Sucrose. *Carbohydrate Research* 1990, *199* (1), 91–109

30. Kuster, B. F. 5-Hydroxymethylfurfural (HMF). A Review Focussing on Its Manufacture. *Starch - Stärke* 1990, *42* (8), 314–321

31. Tang, X.; Zeng, X.; Li, Z.; Hu, L.; Sun, Y.; Liu, S.; Lei, T.; Lin, L. Production of γ-Valerolactone from Lignocellulosic Biomass for Sustainable Fuels and Chemicals Supply. *Renewable and Sustainable Energy Reviews* 2014, *40*, 608–620

32. Saravanamurugan, S.; Nguyen Van Buu, O.; Riisager, A. Conversion of Mono- and Disaccharides to Ethyl Levulinate and Ethyl Pyranoside with Sulfonic Acid-Functionalized Ionic Liquids. *ChemSusChem* 2011, *4* (6), 723–726

33. Saravanamurugan, S.; Riisager, A. Zeolite Catalyzed Transformation of Carbohydrates to Alkyl Levulinates. *ChemCatChem* 2013, *5* (7), 1754–1757

34. Bart, H. J.; Reidetschlager, J.; Schatka, K.; Lehmann, A. Kinetics of Esterification of Levulinic Acid with n-Butanol by Homogeneous Catalysis. *Industrial & Engineering Chemistry Research* 1994, *33* (1), 21–25

35. Zhang, J.; Wu, S. B.; Li, B.; Zhang, H. D. Advances in the Catalytic Production of Valuable Levulinic Acid Derivatives. *ChemCatChem* 2012, *4* (9), 1230–1237

36. Sorokin, A. B. Phthalocyanine Metal Complexes in Catalysis. *Chemical Reviews* 2013, *113* (10), 8152–8191

37. Tolvanen, P.; Sorokin, A.; Mäki-Arvela Päivi; Leveneur Sébastien; Murzin, D. Y.; Salmi, T. Batch and Semibatch Partial Oxidation of Starch by Hydrogen Peroxide in the Presence of an Iron Tetrasulfophthalocyanine Catalyst: The Effect of Ultrasound and the Catalyst Addition Policy. *Industrial & Engineering Chemistry Research* 2011, *50* (2), 749–757

38. Kruid, J.; Fogel, R.; Limson, J. Unsubstituted Metallophthalocyanine Catalysts for the Removal of Endocrine Disrupting Compounds Using H_2O_2 as Oxidant. *Environmental Science and Pollution Research* 2018, *25* (32), 32346–32357

39. Weber, J. H.; Busch, D. H. Complexes Derived from Strong Field Ligands. XIX. Magnetic Properties of Transition Metal Derivatives of 4,4',4",4'"-Tetrasulfophthalocyanine. *Inorganic Chemistry* 1965, *4* (4), 469–471

40. Kadish, K. M.; Dini, D.; Hanack, M. Physical Properties of Phthalocyanine Based Materials. *Phthalocyanines: properties and materials*; Academic Press: San Diego, CA, 2003; Vol. 17

41. Soderberg, T. 2.2 Molecular orbital theory: conjugation and aromaticity

42. Kadish, K. M.; Smith, K. M.; Guilard, R.; Sanders, J.; et al. 15. Axial Coordination Chemistry of Metalloporphyrins. *The Porphyrin handbook: inorganic, organometallic and coordination chemistry*; Academic Press: San Diego, CA, 2000; Vol. 3

43. Mack, J.; Kobayashi, N. Low Symmetry Phthalocyanines and Their Analogues. *Chemical Reviews* 2011, *111* (2), 281–321

44. Fukuzumi, S.; Honda, T.; Kojima, T. Structures and Photoinduced Electron Transfer of Protonated Complexes of Porphyrins and Metallophthalocyanines. *Coordination Chemistry Reviews* 2012, *256* (21-22), 2488–2502

45. Silvers, S. J.; Tulinsky, A. The Crystal and Molecular Structure of Triclinic Tetraphenylporphyrin. *Journal of the American Chemical Society* 1967, *89* (13), 3331–3337

46. Nappa, M.; Valentine, J. S. The Influence of Axial Ligands on Metalloporphyrin Visible Absorption Spectra. Complexes of Tetraphenylporphinatozinc. *Journal of the American Chemical Society* 1978, *100* (16), 5075–5080

47. Mbambisa, G.; Nyokong, T. Synthesis and Electrochemical Characterisation of a near Infrared Absorbing Oxo Vanadium(IV) Octapentylthio-Phthalocyanine. *Polyhedron* 2008, *27* (13), 2799–2804

48. Busch, P. M. rep.; U.S. Department of the Interior, Bureau of Mines: Washington, D.C., 1961; pp 1–95

49. Langeslay, R. R.; Kaphan, D. M.; Marshall, C. L.; Stair, P. C.; Sattelberger, A. P.; Delferro, M. Catalytic Applications of Vanadium: A Mechanistic Perspective. *Chemical Reviews* 2018, *119* (4), 2128–2191

50. Wever, R.; van der Horst, M. A. The Role of Vanadium Haloperoxidases in the Formation of Volatile Brominated Compounds and Their Impact on the Environment. *Dalton Transactions* 2013, *42* (33), 11778

51. Robson, R. L.; Eady, R. R.; Richardson, T. H.; Miller, R. W.; Hawkins, M.; Postgate, J. R. The Alternative Nitrogenase of Azotobacter Chroococcum Is a Vanadium Enzyme. *Nature* 1986, *322* (6077), 388–390

52. Sippel, D.; Einsle, O. The Structure of Vanadium Nitrogenase Reveals an Unusual Bridging Ligand. *Nature Chemical Biology* 2017, *13* (9), 956–960

53. Rodriguez-Carvajal, J. FULLPROF: A Program for Rietveld Refinement and Pattern Matching Analysis. *Abstracts of the Satellite Meeting on Powder Diffraction of the XV Congress of the IUCr* 1990 p. 127, Toulouse, France

54. Le Bail, A.; Duroy, H.; Fourquet, J. L. Ab-Initio Structure Determination of LiSbWO6 by X-Ray Powder Diffraction. *Materials Research Bulletin* 1988, *23* (3), 447–452

55. Li, X.; Feng, Y.; Li, C.; Han, H.; Hu, X.; Ma, Y.; Yang, Y. One-Step Preparation of Metal-Free Phthalocyanine with Controllable Crystal Form. *Green Processing and Synthesis* 2021, *10* (1), 95–100.

56. J.Janczak CCDC 118412: Experimental Crystal Structure Determination, 2000, DOI: 10.5517/cc3z6r0

57. Ziolo, R. F.; Griffiths, C. H.; Troup, J. M. Crystal Structure of Vanadyl Phthalocyanine, Phase II. *Journal of the Chemical Society, Dalton Transactions* 1980, No. 11, 2300.

58. Pakhomov, G. L.; Travkin, V. V.; Luk'yanov, A. Y.; Stakhira, P. I.; Kostiv, N. V. Thin-Film Photovoltaic Cells Based on Vanadyl Phthalocyanine and Fullerene. *Technical Physics* 2013, *58* (2), 223–230

59. Brown, T. L.; LeMay, H. E.; Bursten, B. E.; Murphy, C. J.; Woodward, P. M.; Stoltzfus, M. W.; Lufaso, M. W. *Chemistry: The Central Science*; Pearson: Harlow (UK), 2018.

60. Ziminov, A. V.; Ramsh, S. M.; Terukov, E. I.; Trapeznikova, I. N.; Shamanin, V. V.; Yurre, T. A. Correlation Dependences in Infrared Spectra of Metal Phthalocyanines. *Semiconductors* 2006, *40* (10), 1131–1136.

BIOGRAPHICAL SKETCH

Juan Ricardo Luna was born in 1987 in Brownsville, Texas. He grew up and attended high school in Los Fresnos, Texas. Juan graduated from Los Fresnos High School in the Spring of 2006. He attended the University of Texas at Brownsville pursuing a Bachelor of Science in Chemistry in Fall 2006 but did not complete the degree. As a returning student in the Fall 2015, he was accepted and attended the University of Texas at Rio Grande Valley. Mr. Luna graduated in the Spring of 2018 with a Bachelor of Science in Chemistry and minor in Biology. Continuing his education and career goals, Juan began a Master of Science in Chemistry degree in the Fall of 2018 while he engaged in research, worked as a graduate teaching assistant and attended the curriculum outlined by the degree. He graduated with a Master of Science in Chemistry in August of 2021. Mr. Luna's permanent address is 32167 State Hwy. 100, Los Fresnos, Texas 78566 and email address is luna7683@gmail.com.